AD NUMBER

ADB000285

LIMITATION CHANGES

TO:

Approved for public release; distribution is unlimited.

FROM:

Distribution authorized to U.S. Gov't. agencies only; Administrative/Operational Use; JUN 1974. Other requests shall be referred to Supersonic Transport Office, FAA, Washington, DC.

AUTHORITY

FAA ltr, 26 Apr 1977

Report No. FAA-SS-73-16

SST Technology Follow-On Program—Phase II

FLUTTER ANALYSIS OF AN ALL-MOVABLE HORIZONTAL TAIL WITH GEARED ELEVATOR ON A SUPERSONIC TRANSPORT

Jerry L. Stelma

Boeing Commercial Airplane Company
P.O. Box 3707
Seattle, Washington 98124

D6-60293
June 1974

FINAL REPORT

Task V

Prepared for

FEDERAL AVIATION ADMINISTRATION

Supersonic Transport Office
800 Independence Avenue, S W
Washington, D C 20590

The contents of this report reflect the views of the Boeing Commercial Airplane Company, which is responsible for the facts and the accuracy of the data presented herein. The contents do not necessarily reflect the official views or policy of the Department of Transportation. This report does not constitute a standard, specification, or regulation.

(12) 60 p.

TECHNICAL REPORT STANDARD TITLE PAGE

(19)		
(18) 1. Report No. FAA-SS-73-16	2. Government Accession No.	3. Recipient's Catalog No. (17)
4. Title and Subtitle (6) SST TECHNOLOGY FOLLOW-ON PROGRAM—PHASE II Flutter Analysis of an All-Movable Horizontal Tail With Geared Elevator on a Supersonic Transport.		5. Report Date Jun[redacted]74
		6. Performing Organization Code
7. Author(s) (10) Jerry L. Stelma		8. Performing Organization Report No. (14) D6-60293
9. Performing Organization Name and Address Boeing Commercial Airplane Company P.O. Box 3707 Seattle, Washington 98124		10. Work Unit No.
		11. Contract or Grant No. (15) DOT-FA72WA-2893
12. Sponsoring Agency Name and Address Federal Aviation Administration Supersonic Transport Office 800 Independence Avenue S.W. Washington, D.C. 20591		13. Type of Report and Period Covered (9) Final report on Phase 2, Task 5, cover
		14. Sponsoring Agency Code
15. Supplementary Notes		

16. Abstract

This document presents symmetric flutter analyses conducted on the all-movable horizontal tail of the Boeing-designed SST. Interaction effects on flutter speed that are produced by the wing, fuselage, control systems and elevator gear ratio are included. Failure conditions of the horizontal-tail actuators are covered.

(21) Report on SST Technology Follow-On Programs. Phase 2 Task 5.

See also AD-913 365L and AD-B000 286L.

17. Key Words	18. Distribution Statement
Aeroelasticity Dynamics Flutter Stabilizer Supersonic transport (SST)	Approved for U.S. Government only. Distribution of this report outside the U.S. Government must have prior approval of the Supersonic Transport Office.

19. Security Classif. (of this report)	20. Security Classif. (of this page)	21. No. of Pages	22. Price
Unclassified	Unlimited	59	

Form DOT F 1700.7 (8-69)

a 390 145 mt

CONTENTS

FIGURES

TABLES

ABBREVIATIONS AND SYMBOLS

cg	center of gravity
ECSS	electric command and stability system
HSAS	hardened stability augmentation system
i	$\sqrt{-1}$
k	kips, 1000 lb
M	Mach number
S	Laplace operator
T	transfer function
V_D	design dive speed
δ_e	elevator rotation angle
δ_s	stabilizer rotation angle
η	gearing ratio
$\dot{\theta}$	pitch rate
ω	frequency, rad/sec

1.0 SUMMARY

This document summarizes the symmetric flutter analyses conducted on the all-movable horizontal tail of the Boeing-designed SST. The analytical work was completed under contract to the Department of Transportation as a follow-on technology program after SST program cancellation. The horizontal stabilizer was analyzed for flutter instabilities including the interaction effects of the fuselage and wing structure, the airplane control systems, and the elevator gearing ratio.

Results of the analyses are given in sections 4.4 and 5.3. Based on these results, it is concluded that the SST empennage provided adequate margins of safety for flutter for all flight conditions (including failure conditions) except when the stabilizer was blown back due to high aerodynamic loading. It is also concluded that the flutter speed of an all-movable horizontal stabilizer with geared elevator is relatively insensitive to elevator gearing ratio.

The analyses reported in this document incorporated linear representation of some nonlinear and transient control system conditions. Although this is considered adequate to account for first-order effects on flutter speeds, an extension of these analyses to define the nonlinear effects is recommended. Such studies should employ analog-digital (hybrid) computer techniques for the evaluation of transient actuator conditions.

2.0 INTRODUCTION

Following cancellation of the SST Program in 1971, a program was initiated to complete several flutter analyses of the horizontal tail to preserve technical information for design support and development of future airplanes of this general type. The program consisted of completion of the symmetric flutter analyses of the empennage structure of the SST.

The horizontal-tail design incorporated some unique features of interest and importance to future designs of this type. These included (1) an all-movable slab stabilizer with geared elevators, (2) a quadruple-redundant hydraulic actuation system for the horizontal stabilizer, (3) reliance on actuator stiffness rather than surface mass balance for the suppression of flutter, and (4) the possibility that the aerodynamic hinge moments could become large enough to stall, and even back-drive, the stabilizer actuators with a resultant substantial reduction in actuator stiffnesses. Furthermore, it was necessary to account for the response of the active longitudinal control system in the stabilizer flutter analysis.

Initial empennage flutter studies on the SST represented the system as empennage surfaces attached to the aft body, which was cantilevered from the wing rear spar location. Although the stabilizer-elevator structural model was quite detailed, being derived through careful finite-element representation of the structure, the fuselage itself was represented as a beam and the attachment bulkhead structure was in a preliminary stage of design.

While this analytical model was considered adequate for preliminary design evaluation, it did not fully represent the effects on flutter of the wing/body modes in the frequency region of stabilizer flutter. Flutter speed boundaries associated with initial strength design showed significant deficiencies, as illustrated in figure 1. Addition of stiffness to the hydraulic actuators, supporting structure, and stabilizer carry-through structure raised the speeds to acceptable levels when the actuators were in a holding condition, as shown in figure 1, but actuator failure conditions or the transient conditions of stabilizer under command, stalled actuators, or blown-back actuators still produced flutter speed deficiencies. Analog flutter studies were made that carefully simulated the non-linear effects of external loading and control inputs on dynamic stiffness of the actuator system, using quasi-steady aerodynamic forces that produced flutter speeds closely approximating the results of the linear analyses. The nonlinear behavior of the actuator system did not significantly alter the flutter speed boundaries associated with zero structural damping.

Incorporation of a more detailed representation of the body and inclusion of the wing structural and aerodynamic effects in the linear analysis were underway at the time of the SST program cancellation in the spring of 1971. Results of the completion of these studies are reported in this document. An additional study related to elevator gearing effects on the flutter characteristics of the all-movable stabilizer was conducted under the contract and the results are presented.

3.0 ANALYSIS FLOW

Horizontal-stabilizer flutter analyses using free-free airplane modes were conducted with a stiffness matrix reduced to 194 degrees of freedom representing the symmetric half-airplane. This stiffness matrix was combined with mass data representing three gross-weight conditions to determine normal modes and frequencies for those cases. All horizontal-stabilizer actuators were initially represented as rigid links.

Previous studies of the analytical model employing a cantilevered aft body/horizontal tail indicated that a minimum of six stabilizer modes were required for an accurate flutter solution. Approximately 40 airplane modes (depending on airplane gross weight) were required in order to cover the frequency range of the first six stabilizer modes.

Inspection of the calculated mode shapes indicated that a few modes, particularly at the higher frequencies and heavier weight conditions, were not accurately representing the structure; i.e., individual mass resonances ("tentpoles") appeared in local areas of the wing. These "tentpoles" resulted from the necessity of distributing the mass data over a limited number of nodes.

Alternate mass redistributions over limited areas (so that the airplane cg was not changed) proved to be beneficial in eliminating the "tentpoles" in a number of cases. Those modes associated with the remaining "tentpoles" were dropped from the analyses as being invalid and not representative of the actual structure.

After a representative set of mode shapes and frequencies was obtained for each weight condition, generalized aerodynamic forces were determined at one supersonic and one subsonic Mach number for each weight condition. Three-dimensional, compressible aerodynamic theories (ref. 1 and 2) were used at $M = 0.9$ and 1.65. Flutter solutions including V-g and V-ω plots were then obtained for these conditions. The number of modal degrees of freedom in these solutions ranged from 34 for the lightweight airplane to 40 for the heavyweight airplane.

These analyses served to determine which of the three weight conditions analyzed was critical from a flutter speed standpoint. From these results it was decided to continue the flutter studies for only one weight condition, namely the 417,400-lb gross-weight airplane.

Studies were conducted to determine the necessary modes to be included in the remaining analyses (deleting modes that had no influence on the critical flutter condition). The primary objective was to reduce computer time requirements when generalized aerodynamic forces were calculated for other Mach numbers. The major requirement of the retention studies was to minimize any change in the stabilizer flutter speeds. The flutter speed for the basic wing was more sensitive to modal deletions than the stabilizer mode, with the result that the final set of retained modes produced a moderate change in wing flutter speeds in some cases, although the basic wing flutter mode and its coupling characteristics were essentially unchanged in all analyses.

Results of the modal retention studies showed that 18 modes of the airplane were required supersonically and 26 modes subsonically to accurately assess the horizontal-stabilizer flutter characteristics. Additional flutter analyses were then conducted at M = 0.6, 1.2, and 2.1.

To assess the control-system effects on horizontal-stabilizer flutter, the following steps were taken. The aerodynamic stiffness and damping coefficients were determined for several reduced frequencies in the usual manner. The flutter equations were rewritten in terms of the Laplace transform, S, and merged with the additional actuator-mode and control equations. The merged equations were then solved. The only valid roots of the solution occur when $S = i\omega$, and the locus of these roots (as iterations were made on the reduced frequencies) determined the neutral stability (flutter point). The details of this formulation are given in appendix A. By changing the transfer function (stiffness) of the horizontal-stabilizer actuators, various actuator operating conditions such as holding, stalled, blown-back, etc., were readily assessed.

Evaluation of the failed-actuator conditions was accomplished in the same manner as for the nonfailed conditions. The free-free airplane stiffness matrix was modified by removing the link representing the outboard actuators. New modes were calculated and the analyses proceeded in a manner similar to that for the nonfailure configuration.

4.0 FREE-FREE AIRPLANE ANALYSIS

4.1 DESCRIPTION OF STRUCTURE

The general configuration of the USA supersonic transport is shown in figure 2. The stiffness matrix used for the empennage flutter studies was determined from a finite-element representation of the symmetric half-airplane, using beam and plate elements. Figure 3 shows the horizontal-stabilizer representation. Initially, over 2000 nodes were used to represent the airplane structure. These nodes were chosen to provide the greatest detail possible in representing the empennage structure; to avoid excessive computational requirements some simplifications were required in representing the forward fuselage and wing structure. The basic dynamic characteristics of the wing and forward fuselage were not significantly altered by these simplifications. The representation employed 194 nodes, distributed as follows:body, 19; wing, 46; engine nacelles, 12; horizontal stabilizer, 68; fin and ventral surface, 49.

The horizontal-stabilizer structure was of skin-spar-rib construction in the main box area with full depth honeycomb at the leading edge, tip, and elevator. Figure 4 shows the stabilizer structural configuration. Also shown in figure 4 is a schematic representation of the elevator gearing design.

4.2 DESCRIPTION OF CONTROL SYSTEM

The complete longitudinal flight control system is shown schematically in figure 5 (reproduced from reference 3, where it is explained in more detail). Commands were transmitted from the pilot's controls by mechanical linkage and cables to the master servo was connected mechanically to the control valves on the four stabilizer actuators. Pitch commands were also transmitted electrically via four-channel HSAS (Hardened Stability Augmentation System) and ECSS (Electric Command and Stability System) paths to the four electric command (EC) servos. The output of the EC servos was mechanically summed with the output of the master servo at each surface actuator. Multiple load paths were provided from the master servo to the four stabilizer actuators. Each of the four actuators was powered by a separate, independent hydraulic system. The flight control system used in the flutter analyses is shown in the simplified block diagram of figure 6.

The SST all-movable horizontal stabilizer, chosen for its high degree of control effectiveness, was constrained against rotation solely by the stiffness of the actuation system. Figure 7 shows a typical actuator installation. The stiffness of the full-scale actuation system was determined in an experimental program and reported on in the Phase I SST Technology Follow-On program (ref. 3). The results of these tests were incorporated in the flutter analyses reported herein. Figures 8 and 9 show the magnitude of stiffness and the phase of actuator reaction force relative to actuator deflection when an oscillatory load is applied to the output end of a single horizontal-stabilizer actuator under normal holding conditions.

The SST horizontal-stabilizer design was such that the surface hinge moments were large enough to stall the actuators under certain extreme boundary emergency flight conditions, resulting in a significant decrease in actuator stiffness. The stiffness decrease results from the main servo valve being wide open, thus allowing relatively long hydraulic lines to become the dominant elastic element in the system. The actuator stiffness under stalled conditions, as determined in reference 3, is shown in figure 10. The phase shift is shown in figure 11.

A possibility existed that an extreme airplane maneuver in atmospheric turbulence could produce forces that would exceed actuator capability. Under this condition, the actuators would be driven back from their commanded position, resulting in a significant decrease in actuation system stiffness. Both the main servo valve and the relief/bypass valves are open under blowback conditions. The actuator stiffness and phase shift under blowback conditions, as determined by the reference-3 test, are shown by the solid lines in figures 12 and 13. This drastically reduced stiffness was of major concern during the design of the SST since it produced a statically divergent mode at extremely low speeds. Immediately prior to the SST program cancellation one alternate design, involving a time-delayed bypass valve operation, was presented for flutter evaluation. Its transfer function is shown by the dashed lines in figures 12 and 13. Results of the actuator stiffness tests of reference 3 are reflected in the flutter studies of this document, with the exception of the proposed alternate design, which was not checked during the full-scale hardware test of Phase I.

For high command rates the stabilizer main servo valve is nearly wide open, (i.e., is at approximately the valve opening for the stalled actuator position). At low command rates the main servo valve is nearly closed, (i.e., is at approximately the valve opening for the holding actuator position). Since the under-command stiffness is bounded by two stabilizer operating conditions (stalled and holding) that were analyzed fully, no analyses were conducted for under-command conditions.

4.3 DESCRIPTION OF WEIGHT CONDITIONS

Paneled weights data for three configurations were employed initially, representing airplane gross weights of 417,400, 529,900 and 601,900 lb. The weight conditions also represent a range of center-of-gravity locations approaching fore and aft extremes of expected flight conditions for the airplane. Table I presents weight condition detail.

Of particular concern in the empennage flutter studies was the fact that the SST design incorporated an aft body fuel tank (designated 8A). Previous empennage flutter studies on the SST had indicated that the fuel level in this tank could have a significant effect on the empennage flutter speeds. The location of this tank in relation to the empennage structure is shown in figure 4.

4.4 ANALYSIS RESULTS

4.4.1 Stabilizer Holding Conditions

The three airplane gross weight conditions were initially analyzed for flutter at M = 0.9 and 1.65 with actuators considered to be rigid links and without control system effects

TABLE 1.–AIRPLANE WEIGHT CONDITION DESCRIPTIONS

Wt. condition		Gross weight kips	Center of gravity		Landing gear	Ballast		% fuel	
								Tank no.	
Name	No.		Body station	% C_R		Fwd limit	Aft limit	Main 1	Main 2
Emerg. descent fwd limit	T33	529.9	2095.5	53.0	up	✓		81.2793	84.6457
Nominal climb aft limit	T41	601.9	2158.5	58.2	up		✓	69.9380	72.8346
Nominal descent aft limit	T50	417.4	2158.5	58.2	up		✓	29.0589	30.2625

Wt. condition		% fuel							
		Tank no.							
Name	No.	Main 3	Main 4	1AF-6AF	1AA-6AA	7AF	7AA	8A	2AA-5AA
Emerg. descent fwd limit	T33	90.1140	88.9778	0	0	12.6486	42.4102	0	0
Nominal climb aft limit	T41	77.5400	76.5623	100	100	71.7050	37.1701	90.6285	0
Nominal descent aft limit	T50	32.2175	31.8113	0	0	0	0	39.6499	0

included. Additional analyses were conducted at M = 0.6, 1.20 and 2.1 to complete the curves of figure 14. Similar analyses were run for all three weight conditions with the actuator dynamic properties of figures 8 and 9 included. The results are shown in figure 15. The flutter speeds are somewhat lower than for the rigid-link cases but have the same general trend. The flutter speeds for the empennage as a part of the full airplane are substantially higher than for the cantilevered body representation of figure 1; as a consequence, for the stabilizer holding condition the flutter margins are ample. This is believed to be partly the result of the use of updated versions of the aerodynamics of references 1 and 2 and partly the result of the use of a more detailed mathematical model of the fuselage structure, including the interface between horizontal tail and body. Flutter studies of elevator gear-ratio effects, section 5.0, employed a cantilevered body representation that included the detailed mathematical model of the aft body and stabilizer attachment. These results agreed very well with the full-span data, indicating that the wing/forebody did not change the stabilizer flutter speeds significantly. The significant change in flutter speed from the earlier studies in spite of relatively minor changes in structural representation is believed to be due to inaccuracies in unsteady aerodynamic theory. This emphasizes the need for experimental verification of analytical results for configurations of this type.

4.4.2 Selection of Critical Weight Condition

At M = 0.9, the lightweight airplane condition (417,400 lb) produced the lowest flutter speeds, as shown in the upper graph of figure 16. However, when considering the flutter margin available over 1.15 V_D, shown by the open symbols of the lower graph, the intermediate gross weight configuration (529,900 lb) was critical by a small amount. The flutter characteristics and modal coupling of the 417,400- and 529,900-lb conditions were very similar.

As shown in figure 15 the lightweight and heavyweight configurations had virtually identical flutter speeds at M = 1.65. Thus, at supersonic speeds, the 601,900-lb configuration was somewhat more critical than the 417,400-lb weight condition because of the more stringent flight placard. However, the overall similarity in the characteristics of flutter of the horizontal tail for the range of gross weights studied led to the conclusion that one weight condition was probably sufficient for further flutter studies of control system variations.

Previous studies on an analytical model with a cantilevered aft body and horizontal tail indicated that the lowest stabilizer flutter speeds occurred when the aft fuel tank 8A (fig. 4) was partially full. The data shown in figure 17 for M = 0.9 for the full span case was in agreement with these previous results. This led to the selection of the 417,400-lb configuration for further studies.

4.4.3 Actuator Failure and Extreme Loading Conditions

The potential reduction in flutter speed associated with failure of the outboard actuators and also with loss of stiffness under blow-back and stalled actuator conditions described in section 4.2 was investigated using the 417,400-lb configuration.

4.4.3.1 Failed Outboard Actuators

Figure 18 shows the flutter speeds for the condition where the outboard actuators are failed and the inboard actuators are rigid. The flutter speed boundary and modal coupling for the failure case are very similar to the nonfailure case, indicating little effect from the loss of the outboard links.

When the actuators and associated control system are substituted for the inboard links (i.e., when the transfer functions of figs. 8 and 9 are used), the flutter boundaries become as shown in figure 19. Two significant changes in the flutter characteristics are seen by comparing figure 19 with the rigid-actuator configuration of figure 18. First, the critical flutter mode is now the first body-bending mode, both subsonically and supersonically. Second, a considerable decrease in flutter speed has resulted, again most significantly in the supersonic regime. There remains, however, adequate actuator stiffness to prevent stabilizer flutter within the design flight placard, which is V_D for the failure case.

4.4.3.2 Stalled Actuators

Figure 20 shows the flutter boundary when the stalled-actuator transfer function (figs. 10 and 11) is coupled with the elastic equations of motion. The stabilizer flutter characteristics are similar to the actuator-failure condition in that the critical flutter mode originates as the first body-bending mode throughout the Mach regime. The stalled-actuator transfer function exhibits low stiffness in the flutter frequency region, thus resulting in considerably reduced flutter speeds. Figure 20 shows that the flutter boundary is, however, above the design flight placard for all Mach numbers.

4.4.3.3 Blown-Back Actuators

The blown-back transfer function of the reference 3 tests was known to produce an extremely low static divergence and therefore was not analyzed in detail for all flight conditions. The proposed blown-back fix was an attempt to remedy the divergence condition; the transfer function for it is shown in figures 21 and 22. As can be seen, the transfer function is of the sixth order and as such was beyond the capabilities of the flutter solution computer program to use explicitly.

An approximation to the proposed blown-back fix transfer function was developed with a second-order transfer function as shown in figures 21 and 22. Since the flutter frequencies are in the 7.5- to 9.5-rad/sec range, it is felt that the approximate second-order transfer function represents the proposed sixth-order transfer function satisfactorily for this blown-back analysis.

The second-order transfer function was then coupled with the elastic equations of motion, the result being the flutter boundary shown in figure 23. Again, the critical flutter mode originated as the first body-bending mode.

The proposed blown-back fix transfer function still does not possess adequate stiffness to prevent flutter in the supersonic regime, although it offers a significant improvement over the static divergence situation produced by the reference-3 transfer function. It is likely that

modification of the system to decrease the actuator phase angle would substantially aid in providing flutter clearance.

4.5 NATURAL MODES AND FREQUENCIES

Table 2 summarizes the modal frequencies for the three weight conditions analyzed. For these reference mode cases, all horizontal-stabilizer actuators are represented by rigid links. Also noted in the table are those modes retained for the flutter analyses, i.e., those modes that contribute significantly to stabilizer flutter. These mode shapes are plotted and presented in reference 4.

Table 3 presents the modal frequencies for the case with outboard actuators failed compared with the case with all four actuators connected. Again, for these reference cases the actuators are considered to be rigid links. As expected, the modal frequencies for the two configurations are nearly identical except for those modes involving horizontal-stabilizer motion. Reference 4 contains the plotted mode shapes for the two-actuator condition on the lightweight (417,400-lb) airplane.

4.6 FLUTTER VELOCITIES AND FREQUENCIES

Table 4 summarizes the flutter speeds and frequencies for all configurations of the actuator that were analyzed. Of additional interest were the results of two studies made at Mach 0.9 and 2.1 wherein the wing aerodynamic forces were deleted from the flutter solution. Generalized inertia and stiffness contributions were retained, however. Very little change in the horizontal-tail pitch flutter mode was observed; however, the body-bending flutter mode disappeared, leading to the conclusion that wing aerodynamic forces are needed for a thorough assessment of empennage flutter characteristics. Subsequent studies indicated that the body-bending flutter mode was also affected significantly by control system characteristics. Nevertheless, the cantilevered aft-body analyses can provide significant flutter results for preliminary design assessment.

TABLE 2.–MODAL FREQUENCIES FOR SYMMETRIC EMPENNAGE FLUTTER ANALYSES

Free-free airplane modal frequencies (cps)							
Mode	Gross weight, kips			Mode	Gross weight, kips		
	417.4	529.9	601.9		417.4	529.9	601.9
1	0	0	0	21	[a] 11.52	[a] 11.06	[ab] 10.27
2	0	0	0	22	[a] 12.89	[a] 11.15	10.61
3	[ab] 0	0	0	23	[a] 14.04	11.34	[ab] 11.27
4	[ab] 1.452	[a] 1.488	[ab] 1.271	24	[a] 14.33	11.88	11.65
5	[ab] 1.920	[a] 1.836	[ab] 1.673	25	[a] 14.66	12.32	12.03
6	[ab] 2.701	[a] 2.681	2.508	26	[ab] 14.74	12.98	12.40
7	[a] 3.078	[a] 3.047	[ab] 2.958	27	[ab] 14.95	13.88	12.47
8	3.721	[a] 3.512	[ab] 3.412	28	15.26	14.04	12.75
9	3.868	[a] 3.789	3.785	29	15.54	14.42	13.37
10	[a] 4.021	[a] 3.866	3.865	30	15.81	14.53	13.51
11	[ab] 5.268	[a] 4.905	[ab] 4.434	31	16.63	[a] 14.80	14.36
12	[a] 5.710	[a] 5.360	[ab] 5.311	32	[ab] 16.89	[a] 14.82	14.58
13	[ab] 7.002	[a] 6.619	6.034	33	[ab] 17.18	[a] 15.30	14.74
14	[ab] 7.558	[a] 7.545	[ab] 6.786	34	18.09	[a] 15.90	[ab] 14.81
15	[ab] 8.047	[a] 7.906	[ab] 7.103	35		16.40	[ab] 14.96
16	[ab] 9.203	[a] 9.031	[ab] 7.826	36		16.55	[ab] 15.15
17	[ab] 9.478	[a] 9.255	8.514	37			15.34
18	[a] 9.786	[a] 9.442	9.282	38			15.92
19	[ab] 10.67	[a] 9.509	9.506	39			16.31
20	[ab] 11.38	[a] 10.63	[ab] 9.660	40			[ab] 16.54

Note:

[a]Mode retained for subsonic analyses

[b]Mode retained for supersonic analyses

Note: all stabilizer actuators assumed rigid

TABLE 3.–MODAL FREQUENCY COMPARISON FOR SYMMETRIC STABILIZER ACTUATOR FAILURE

Mode	Actuators		Mode	Actuators	
	2 outbd 2 inbd	2 inbd		2 outbd 2 inbd	2 inbd
1	0	0	18	9.786	9.786
2	0	0	19	10.67	10.19
3	0	0	20	11.38	11.38
4	1.452	1.452	21	11.52	11.52
5	1.920	1.920	22	12.89	12.89
6	2.701	2.701	23	14.04	14.04
7	3.078	3.078	24	14.33	14.33
8	3.721	3.721	25	14.66	14.63
9	3.868	3.868	26	14.74	14.73
10	4.021	4.021	27	14.95	14.94
11	5.268	5.267	28	15.26	15.26
12	5.710	5.707	29	15.54	15.54
13	7.002	6.989	30	15.81	15.81
14	7.558	7.536	31	16.63	16.63
15	8.047	7.975	32	16.89	16.89
16	9.203	9.126	33	17.18	17.17
17	9.478	9.450	34	18.09	18.09

Free-free airplane modal frequencies (cps)

Note; rigid actuators; 417,400-lb gross weight airplane

TABLE 4.—SUMMARY OF HORIZONTAL STABILIZER SYMMETRIC FLUTTER ANALYSES USING FREE-FREE AIRPLANE MODES

Airplane gross weight, kips	Actuators operating	Mach no.	Number of degrees of freedom	Flutter velocity, V_f in knots EAS (flutter frequency in cps)											
				Rigid actuators			Holding actuators			Stalled actuators			Blown back actuators		
				Wing	Body bending	Horizontal tail pitch	Wing	Body bending	Horizontal tail pitch	Wing	Body bending	Horizontal tail pitch	Wing	Body bending	Horizontal tail pitch
601.9	All	1.65	40	485 (2.3)	a	735 (1.8)									
601.9	All	0.9	40	430 (2.3)	a	750 (1.8)									
529.9	All	0.9	36	485 (2.5)	663 (1.1)	783 (4.2)									
417.4	All	0.6	26	553 (3.0)	606 (1.4)	762 (4.6)	620(2.9)	586(1.3)	728(2.6)	611(2.4)	528(1.4)	a	651(2.4)	480(1.3)	a
417.4	All	0.9	34	510 (2.5)	617 (1.2)	726 (3.2)									
417.4	All	0.9	26	525 (2.5)	610 (1.2)	733 (3.1)	510(2.4)	595(1.0)	720(1.7)	485(2.4)	595(1.0)	a	497(2.4)	561(1.2)	a
417.4	All	1.20	18	486 (2.5)	a	675 (1.8)	485(2.4)	a	630(1.8)	470(2.3)	562(1.5)	a	465(2.3)	463(1.4)	a
417.4	All	1.65	34	490 (2.5)	a	735 (2.0)									
417.4	All	1.65	18	565 (2.5)	a	740 (2.0)	565(2.5)	a	695(1.8)	525(2.3)	583(1.6)	a	525(2.3)	500(1.5)	a
417.4	All	2.10	18	738 (2.6)	a	905 (2.1)	720(2.6)	a	838(1.9)	668(2.5)	710(1.6)	a	680(2.5)	612(1.5)	a
417.4	Inboard	0.9	34	514 (2.5)	600 (1.2)	714 (3.2)									
417.4	Inboard	0.9	26	526 (2.5)	615 (1.2)	725 (3.1)	433(2.3)	549(1.5)	a						
417.4	Inboard	1.65	18	575 (2.6)	a	735 (2.0)	475(2.4)	582(1.5)	a						
417.4	All	.9	34	ab	ab	[b]725 (3.1)									
417.4	All	2.1	18	ab	ab	[b]883 (2.3)									
601.9	All	.9	17	632 (2.5)	a	750 (2.5)	625(2.3)	a	700(1.8)						
601.9	All	1.65	17	835 (2.9)	a	725 (1.8)	815(2.9)	a	693(1.6)						
529.9	All	.9	26	508 (2.5)	640 (1.1)	790 (4.2)	480(2.4)	620(.9)	725(3.8)						

[a]Does not flutter

[b]Wing generalized aerodynamic forces deleted

5.0 CANTILEVERED AFT BODY ANALYSIS

5.1 DESCRIPTION OF STRUCTURE

A separate study was performed to assess the effect of elevator-gearing ratios upon the flutter speeds of an all-movable stabilizer. The analytical structural model of the fuselage used for these analyses consisted of an idealization of the SST aft body, cantilevered at the wing rear spar. The structural idealization was identical to the corresponding portion of the structure used for the free-free airplane analysis described in section 4.0.

Figure 24 shows schematically how elevator gearing is defined and accomplished. The gearing ratio is nearly constant for small stabilizer rotation angles (i.e., when $\delta_S \approx 0$), but deviates from this value near the design limits for stabilizer rotation (i.e., when $\delta_S \approx \pm 15°$). Normal modes and generalized aerodynamic forces were calculated, however, for elevator gearing at $\delta_S = 0$.

Three gearing ratios were examined for their effect on stabilizer flutter. The SST stabilizer design gearing ratio (η) of 1.77 was analyzed, as well as $\eta = 0$ (no gearing) and $\eta = 2.5$. These gearing ratios were chosen to cover the range of values considered in earlier designs of the SST stabilizer.

Each flutter analysis originated with the generation of new stiffness matrices for the particular gearing ratio being examined. For the non-geared elevator, this preliminary step consisted of removing the structural members representing the actuation arm and link and inserting a localized member to lock the elevator to the main stabilizer structure. Thus, the stabilizer and elevator rotated as a single surface.

A gearing ratio of 2.5 was accomplished by modifying the geometry of the actuation arm and link structure. Figure 25 shows how this was accomplished and shows the resulting change in elevator rotation in comparison with the configuration with the gearing ratio of 1.77.

5.2 DESCRIPTION OF CONTROL SYSTEM

The control system used for the cantilevered flutter analyses was identical to that used in the free-free analyses except that the longitudinal control system loops (ECSS and HSAS) were not included. A block diagram of the control system is shown in figure 26. As was done in the free-free analysis of section 4.0, the horizontal-stabilizer actuators were initially assumed to be rigid links. The control system and actuator mode equations were then merged with the elastic structure equations as described in reference 4. The holding-actuator transfer function of figures 7 and 8 was used when the control system effects were assessed. No analyses were made for the stalled or blown-back actuator conditions.

5.3 ANALYSIS RESULTS

The flutter speed of the horizontal stabilizer with all-movable geared elevator was found to be quite insensitive to the gearing ratio. This was particularly true when rigid actuators were assumed for the stabilizer.

When the actuator control-system effects were included in the analysis, a definite trend was observed which indicated that increasing the gearing ratio tended to increase the flutter speeds. The sensitivity, however, was still quite small, the maximum variation in flutter speeds being on the order of 2.5 percent.

In general, it was observed that decreasing the rotational constraining stiffness (including control-system effects or having failed actuators) tended to make the flutter speeds more sensitive to elevator gearing ratios, with increased gearing ratio producing increased flutter speeds.

5.3.1 Natural Modes and Frequencies

Table 5 shows the modal frequencies for the structural configurations analyzed. Eight modes were used in all flutter solutions. Two airplane design weights (529,900 and 690,300 lb gross) were analyzed in detail in the normal operating condition (all four actuators operating) and in the failure condition (outboard actuators failed). Reference 4 shows the plotted mode shapes for each analysis configuration.

5.3.2 Flutter Speeds and Frequencies

5.3.2.1 Rigid Actuators

Figures 27 and 28 show the rigid actuator flutter results for the configurations both with and without actuator failure, at Mach = 0.9 and 1.65. As can be seen, the flutter speeds appear to be quite insensitive to gearing ratio, the maximum change in flutter speeds only slightly exceeding 1 percent. The trend of the change is not conclusively established.

5.3.2.2 Control System Effects

Including the control system of figure 26 in the flutter analysis for the holding condition appears to amplify somewhat the effect that change of gearing ratio has on flutter speeds. The change in flutter speed due to gearing ratio changes is still small, the maximum variation being on the order of 2.5 percent. Inclusion of the control system also seems to establish a definite trend in the effect of gearing ratio on flutter speed; figures 29 and 30 show that increasing the gearing ratio tends to increase the flutter speeds.

TABLE 5.–MODAL FREQUENCIES FOR GEARED ELEVATOR FLUTTER ANALYSES

Modal frequencies[a] (cps)

Gearing ratio	Mode	529.9 kips		690.3 kips	
		All act. oper.	Outbd act. failed	All act. oper.	Outbd act. failed
0	1	2.37	2.37	1.92	1.92
	2	10.21	9.92	7.85	7.78
	3	12.82	12.48	11.75	11.29
	4	14.76	14.73	14.16	14.05
	5	17.95	17.85	14.71	14.67
	6	20.43	20.39	19.00	18.86
	7	23.80	23.69	20.07	20.07
	8	24.58	24.58	21.72	21.71
1.77	1	2.369	b	1.92	1.92
	2	9.64	b	7.78	7.63
	3	11.85	b	10.60	10.05
	4	14.82	b	13.59	13.56
	5	16.03	b	14.82	14.79
	6	20.05	b	16.67	16.65
	7	23.2	b	20.06	20.06
	8	24.57	b	22.10	22.09
2.5	1	2.37	2.37	1.92	1.92
	2	9.32	8.70	7.73	7.53
	3	11.60	11.50	10.16	9.65
	4	14.77	14.74	13.46	13.44
	5	15.73	15.73	14.82	14.79
	6	20.01	19.99	16.35	16.35
	7	23.15	23.13	20.06	20.06
	8	24.56	24.56	22.12	22.12

[a]All actuators assumed rigid, and fuselage structure cantilevered at wing rear spar
[b]Modes not calculated

6.0 CONCLUSIONS AND RECOMMENDATIONS

The following summarize the conclusions and recommendations of this study:

1) The analyses performed indicate that the SST empennage provides adequate margins of safety for flutter for all flight conditions (including hydraulic actuator failure) except when the stabilizer is blown back due to high aerodynamic loading.

2) The analyses further indicate that the horizontal-tail flutter speeds are relatively insensitive to elevator gearing-ratio changes.

3) Differences in flutter speeds obtained from the analyses conducted under this contract, which employed updated three-dimensional unsteady aerodynamics, and from corresponding analyses completed previously point out the need for experimental confirmation of analytical results for configurations of this sort. It is therefore strongly recommended that tests of the 1/7-scale SST transonic empennage flutter model be conducted to provide a basis for correlation between analysis and test.

4) Although the linear representation of the hydraulic system stiffness used in the analyses is considered to be a satisfactory approach for first-order assessment of flutter characteristics of systems of this type, further work to develop analytical methods that account for hydraulic system nonlinearities is recommended. Such studies should employ analog-digital (hybrid) computer techniques to evaluate transient actuator behavior.

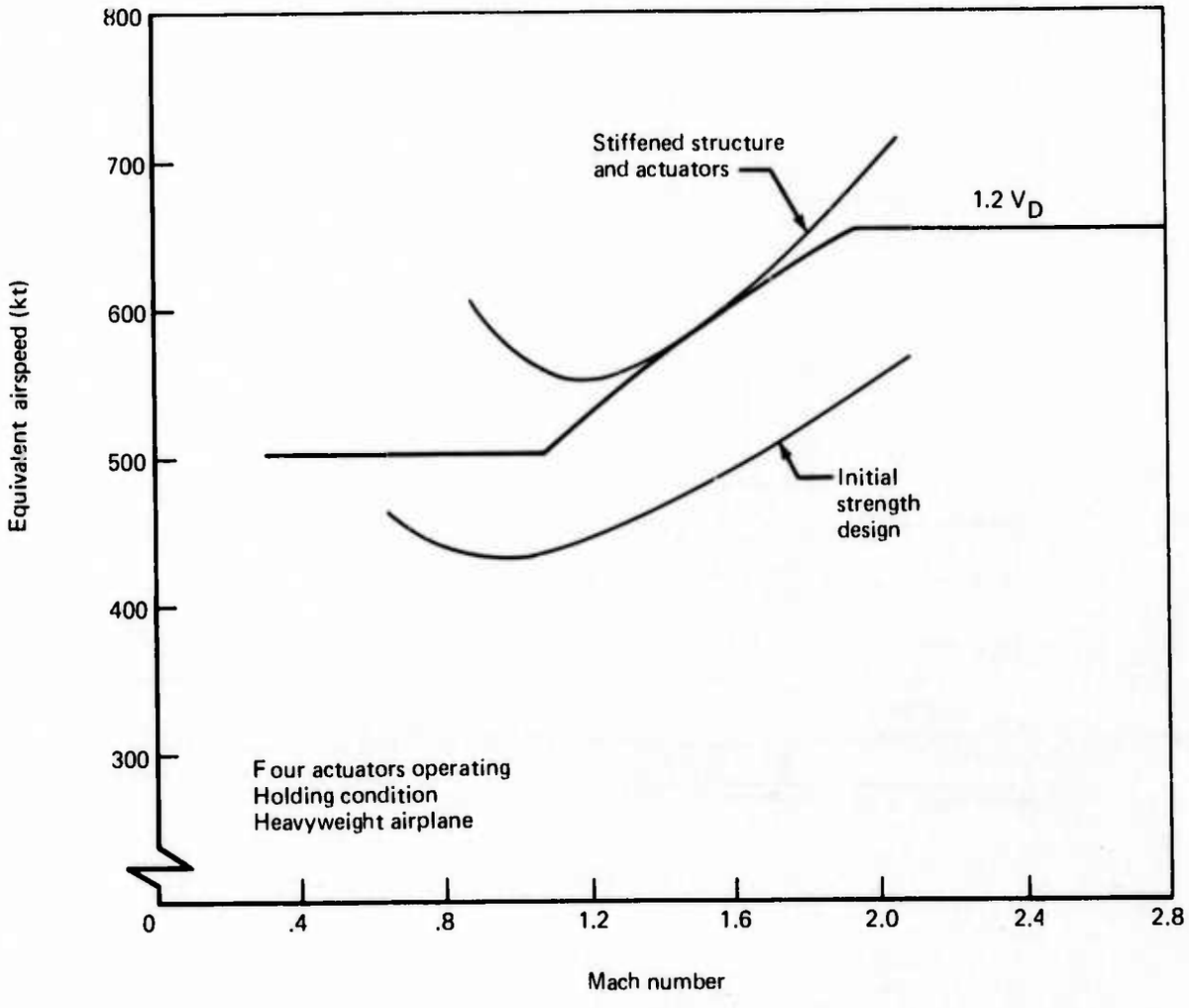

FIGURE 1.–SST STABILIZER FLUTTER BOUNDARY

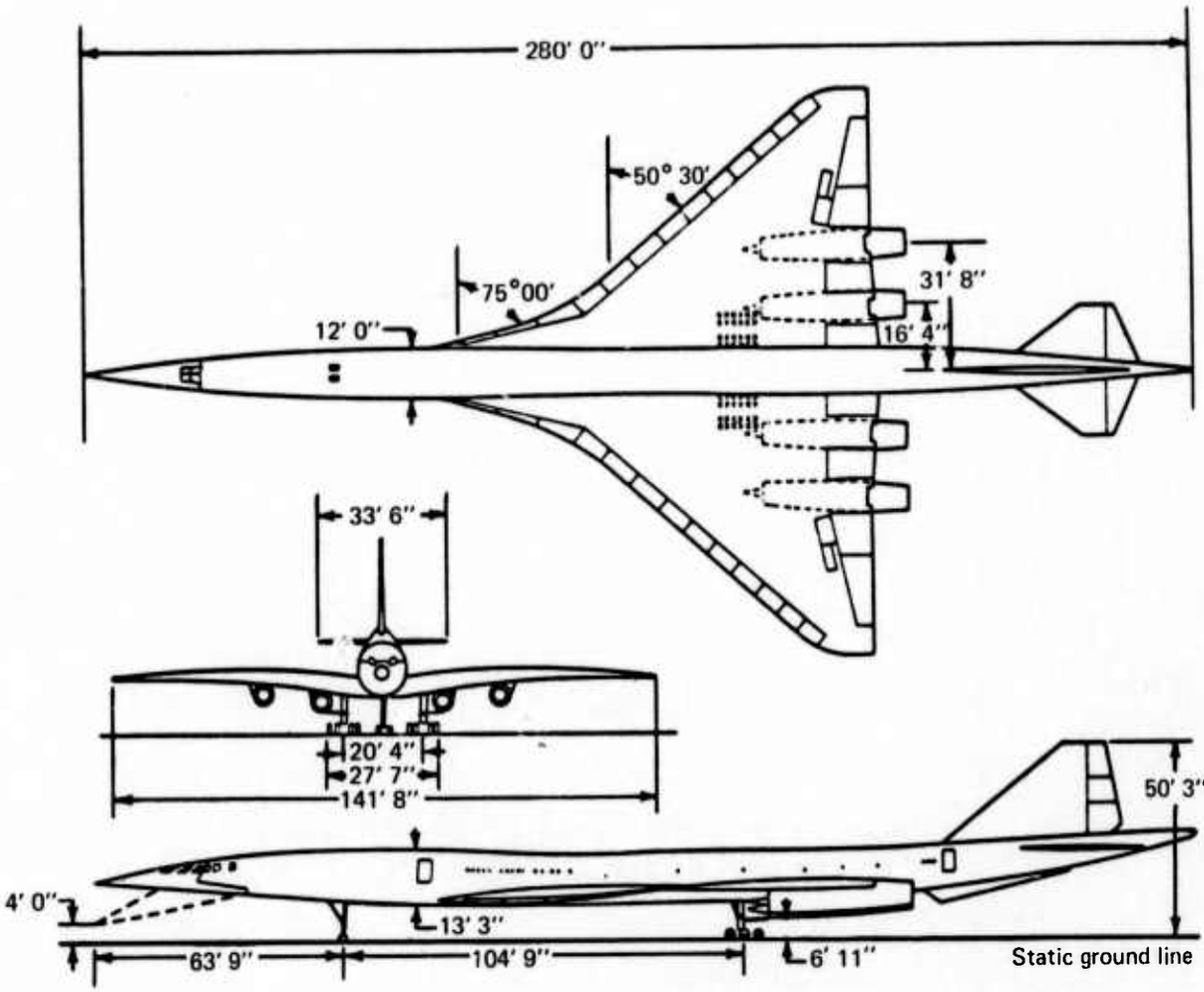

FIGURE 2.–GENERAL CONFIGURATION, USA SST

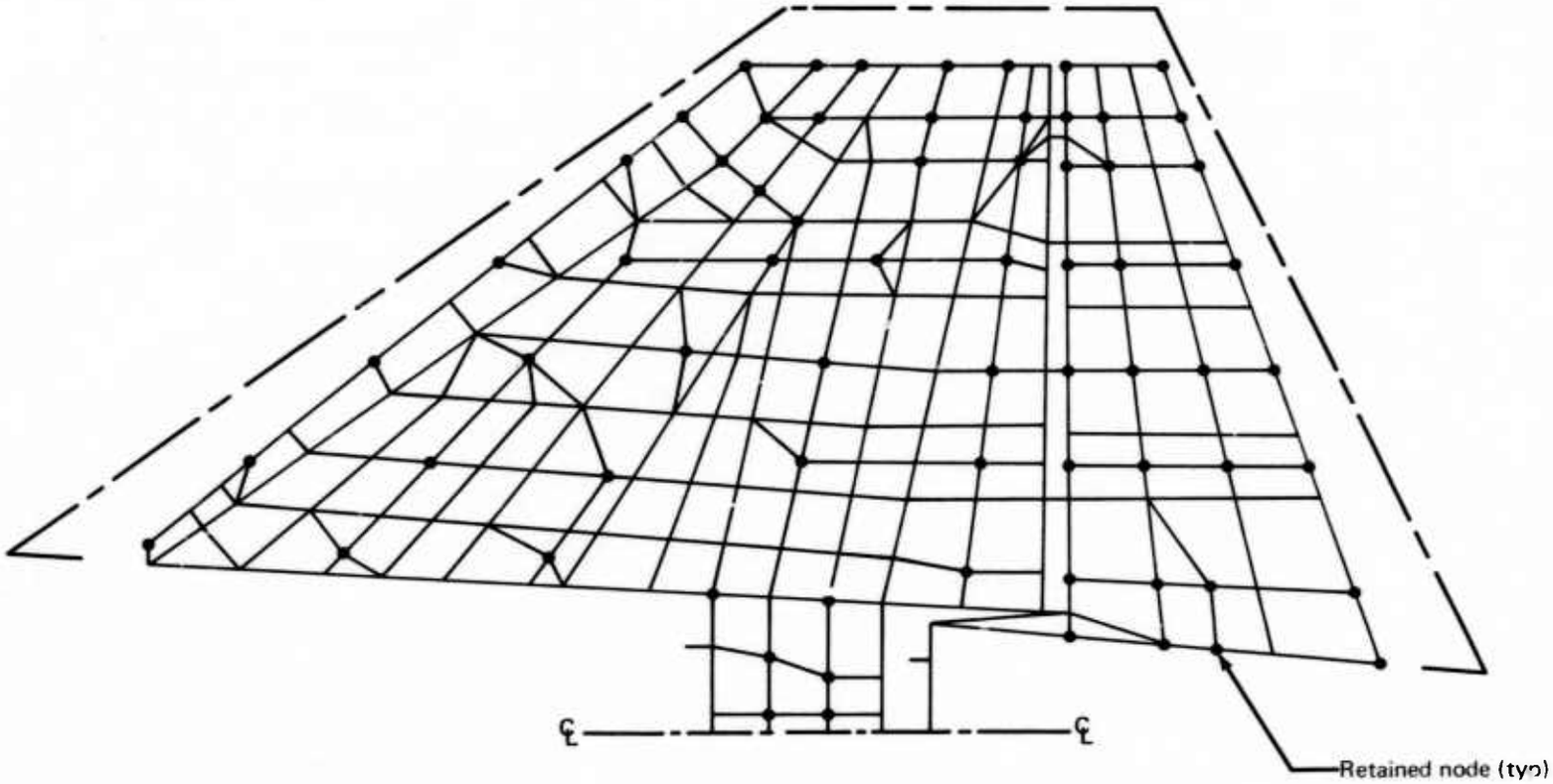

FIGURE 3.–HORIZONTAL STABILIZER STRUCTURAL IDEALIZATION

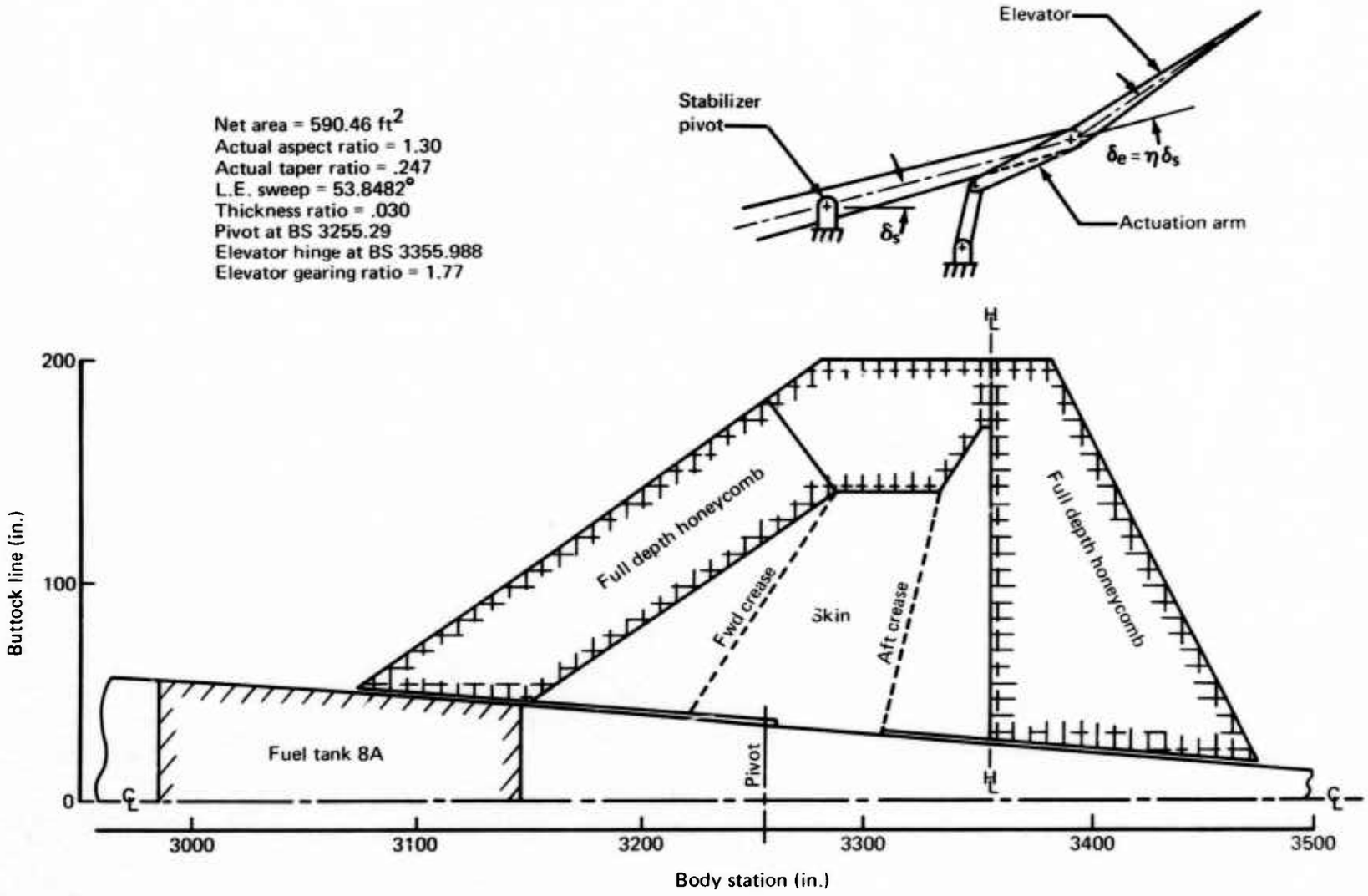

FIGURE 4.–HORIZONTAL STABILIZER STRUCTURAL CONFIGURATION

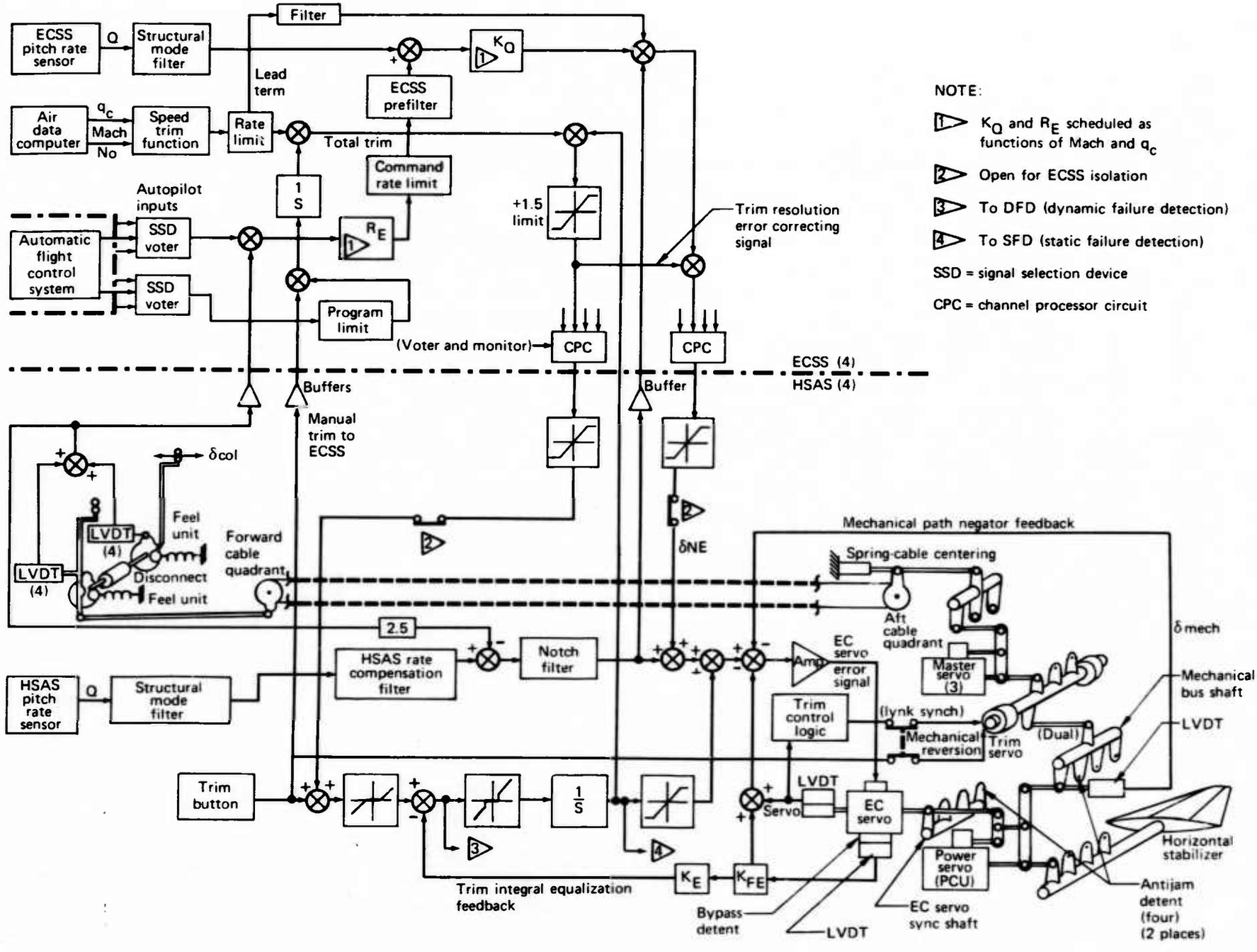

FIGURE 5.–SCHEMATIC OF LONGITUDINAL FLIGHT CONTROL SYSTEM

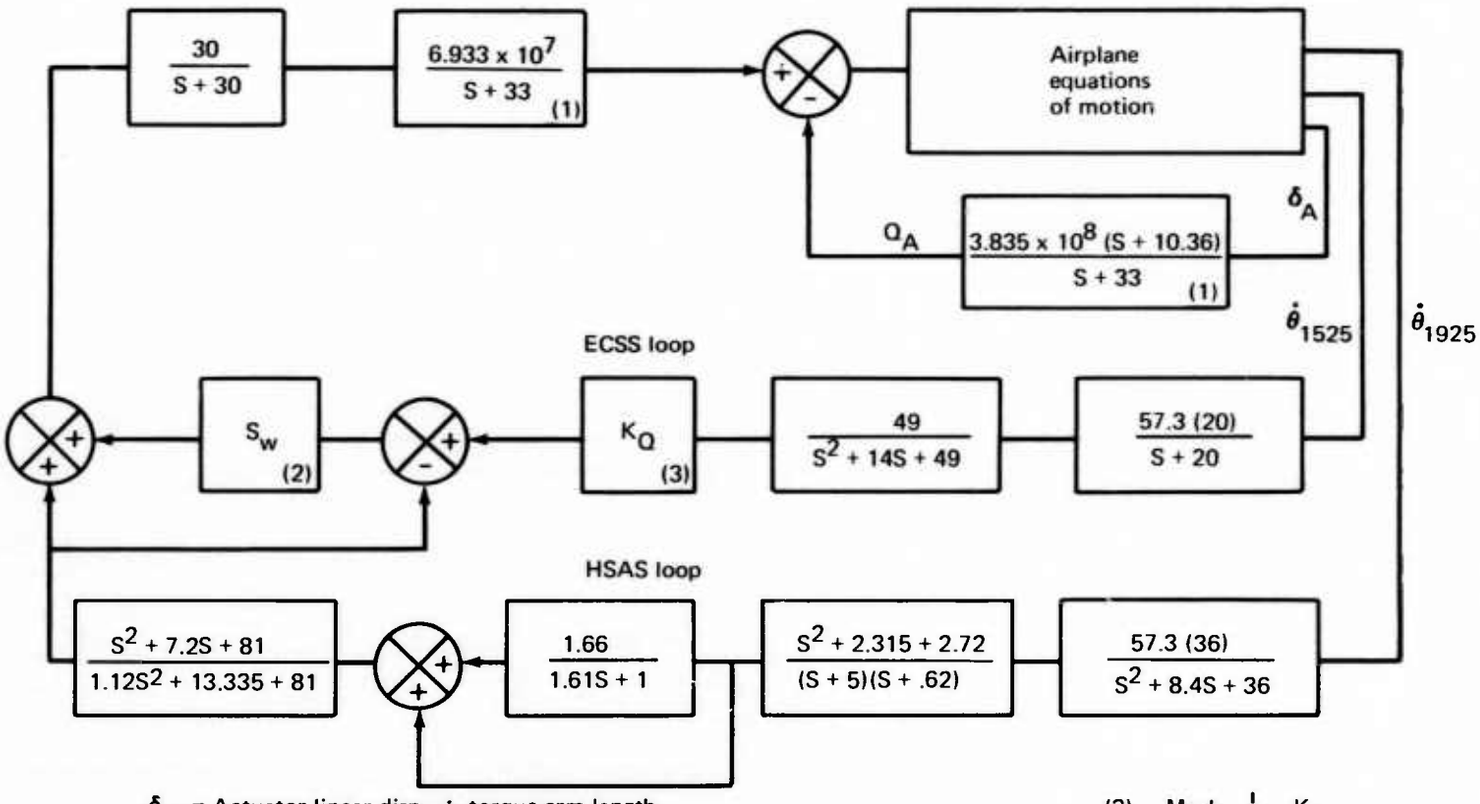

δ_A = Actuator linear disp. ÷ torque arm length

Q_A = Actuator force times torque arm length

$\dot{\theta}_{BS}$ = Pitch rate at body station

(1) Transfer function varies with actuator configuration. Single, holding actuator shown acting at 33.1 in. from hinge ($\delta_s = 0$)

(2) S_w = 1 for ECSS operation
= 0 for HSAS operation

(3)

Mach	K_Q
0.6	.67
0.9	.76
1.20	.60
1.65	.60
2.10	.71

FIGURE 6.—CONTROL SYSTEM AS USED IN FLUTTER ANALYSES

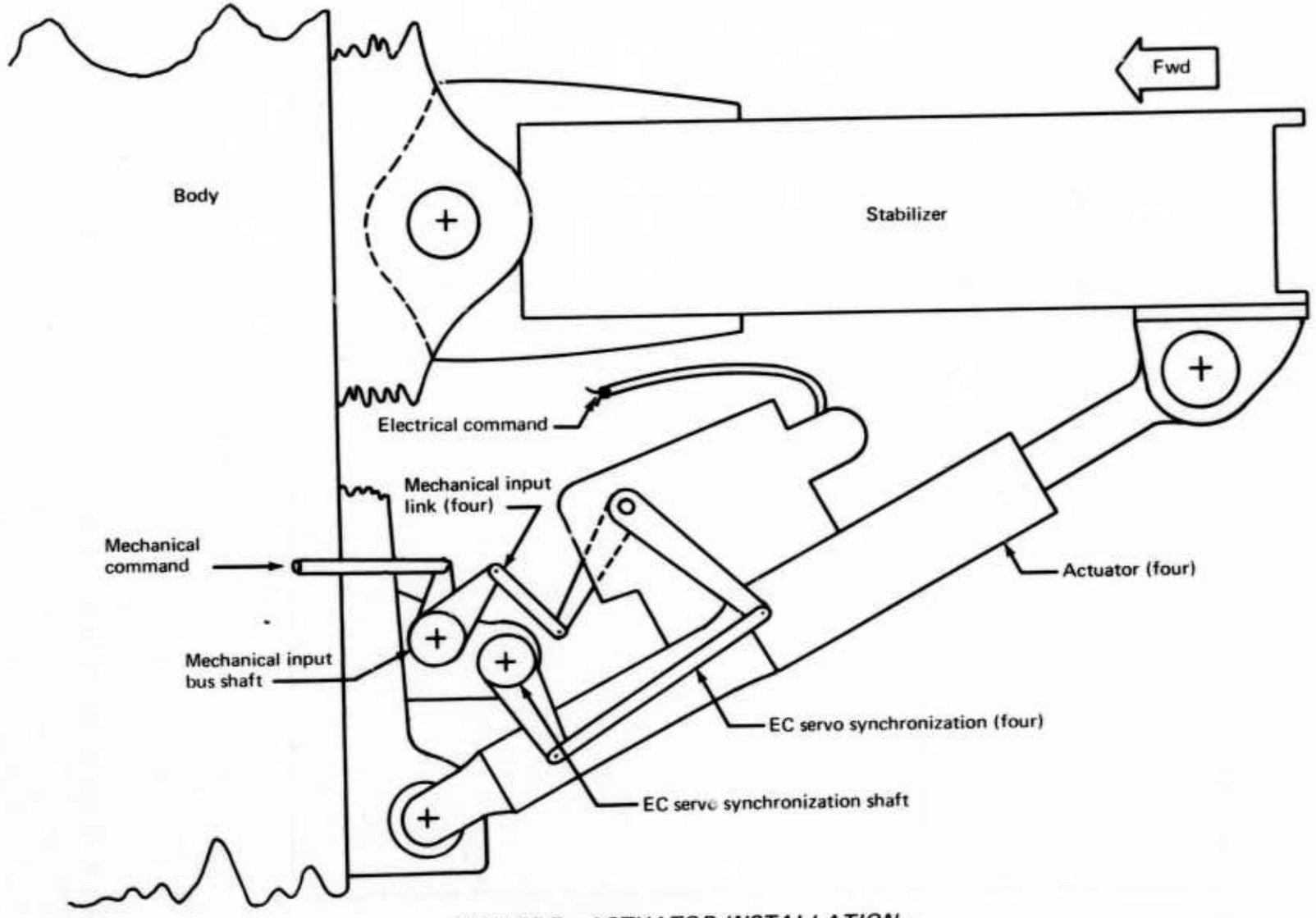

FIGURE 7.–ACTUATOR INSTALLATION

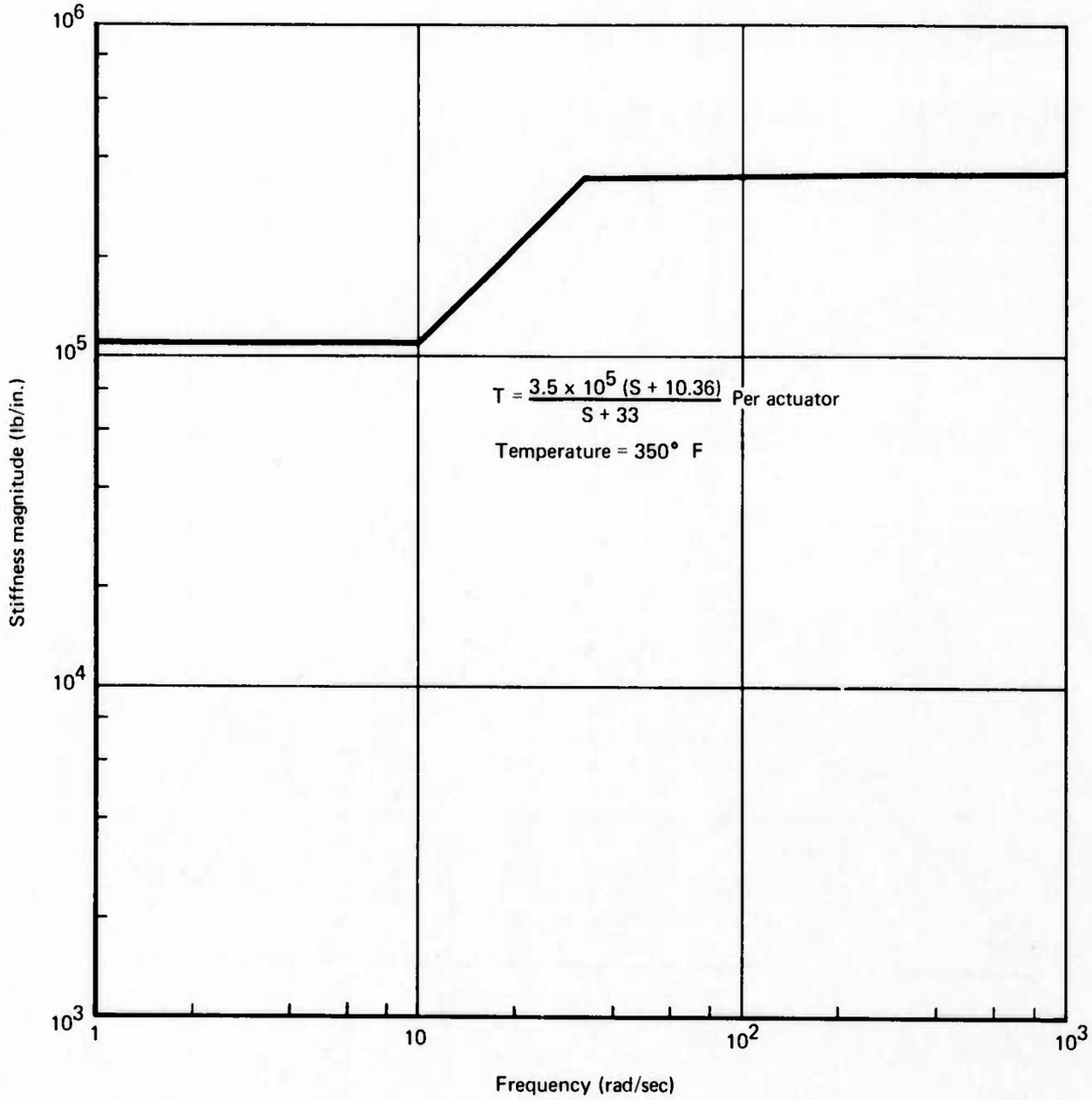

FIGURE 8.--HORIZONTAL STABILIZER ACTUATOR STIFFNESS, HOLDING CONDITION

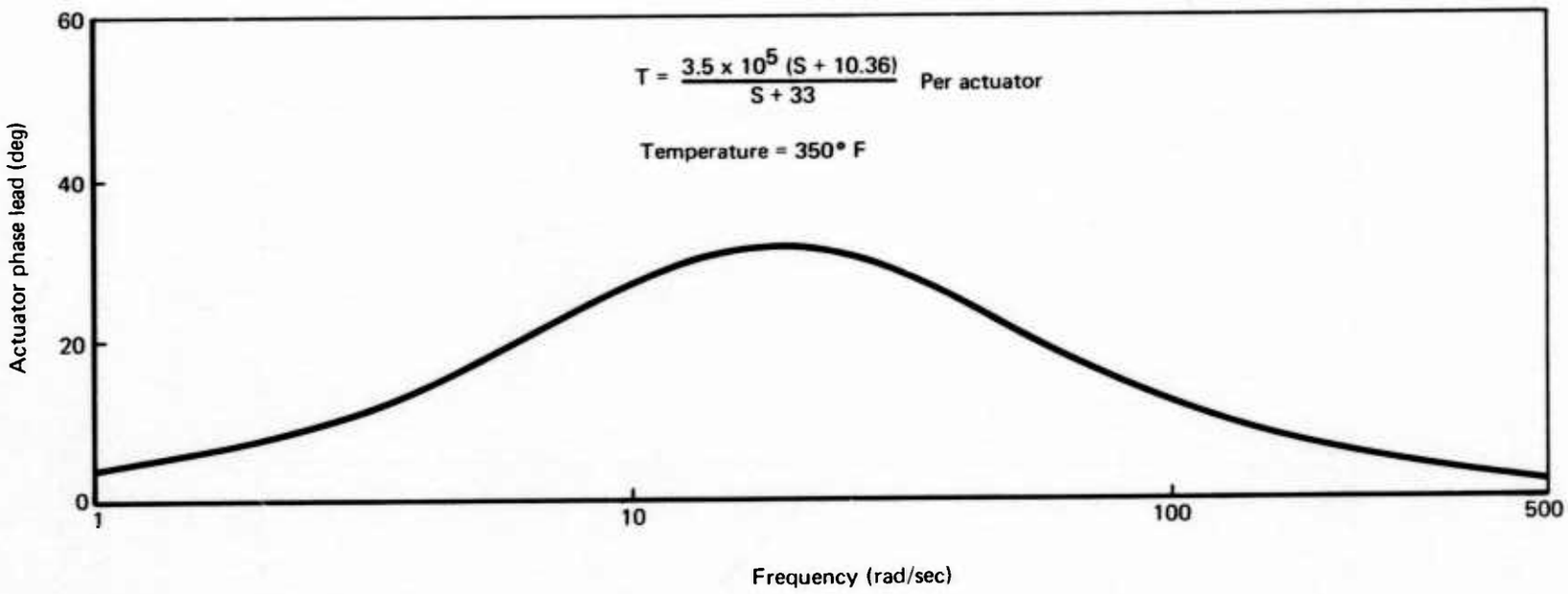

FIGURE 9.—HORIZONTAL STABILIZER ACTUATOR PHASE ANGLE, HOLDING CONDITION

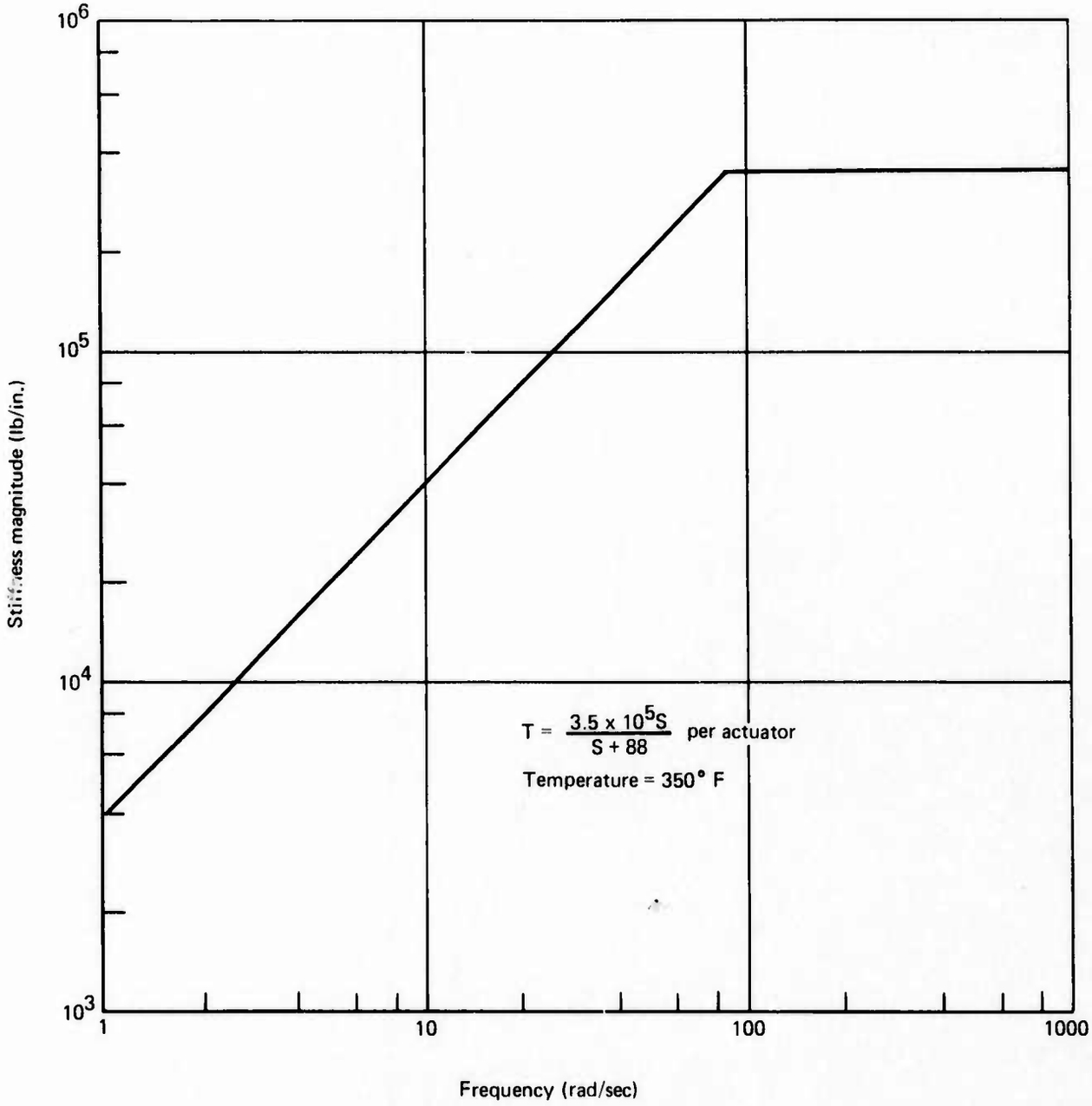

FIGURE 10.–HORIZONTAL STABILIZER ACTUATOR STIFFNESS, STALLED CONDITION

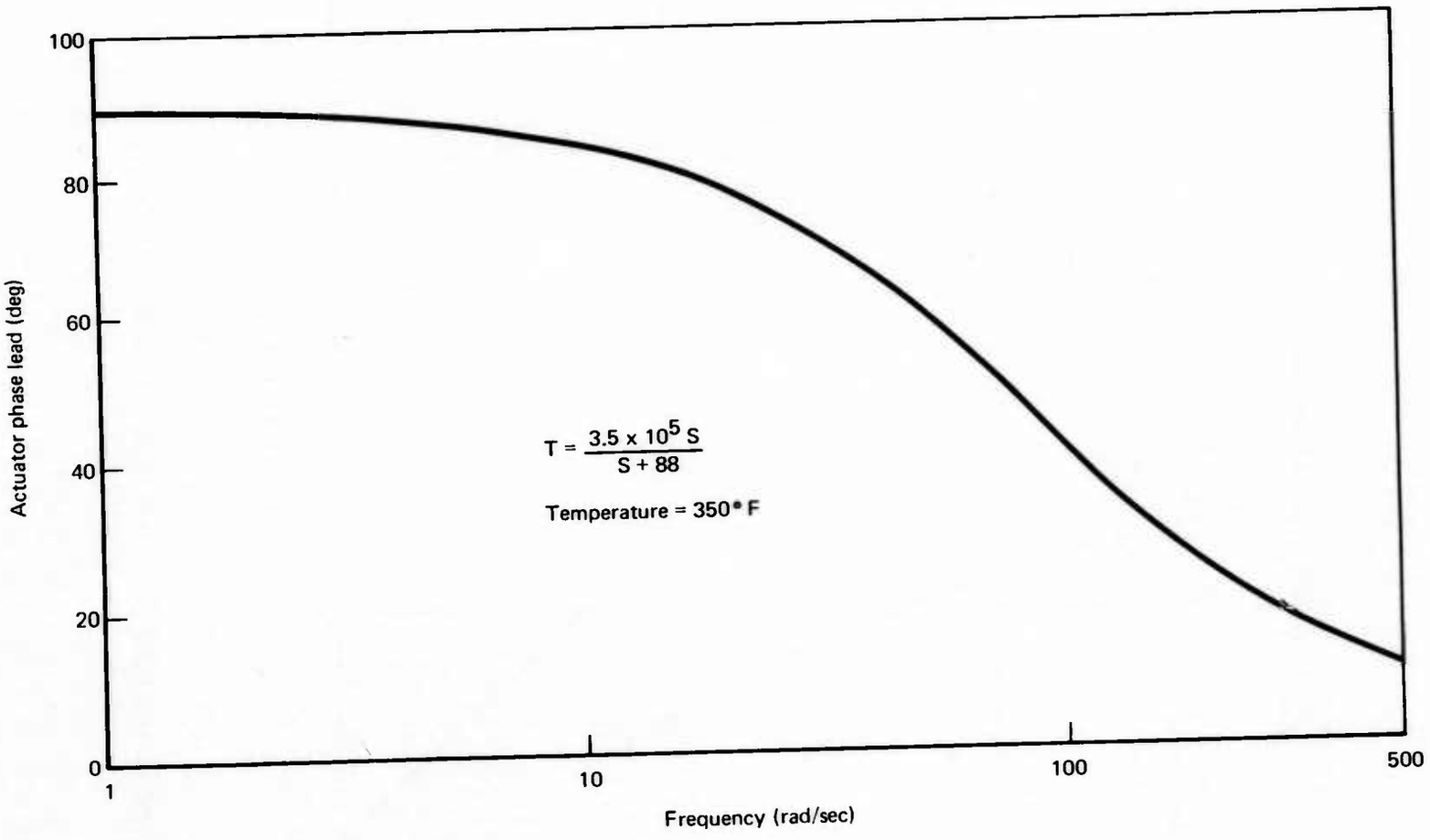

FIGURE 11.–HORIZONTAL STABILIZER ACTUATOR PHASE ANGLE, STALLED CONDITION

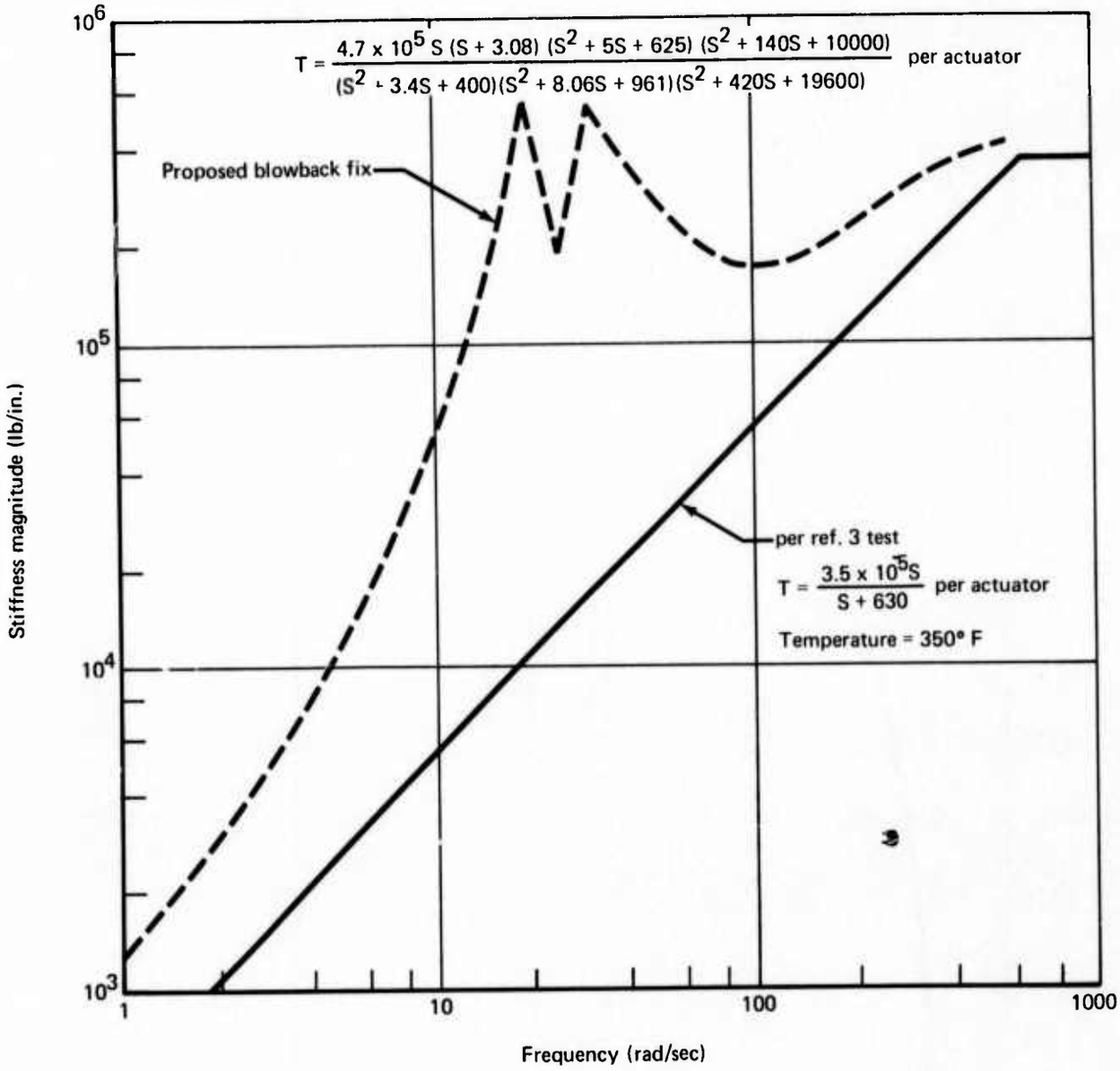

FIGURE 12.–HORIZONTAL STABILIZER ACTUATOR STIFFNESS, BLOWBACK CONDITION

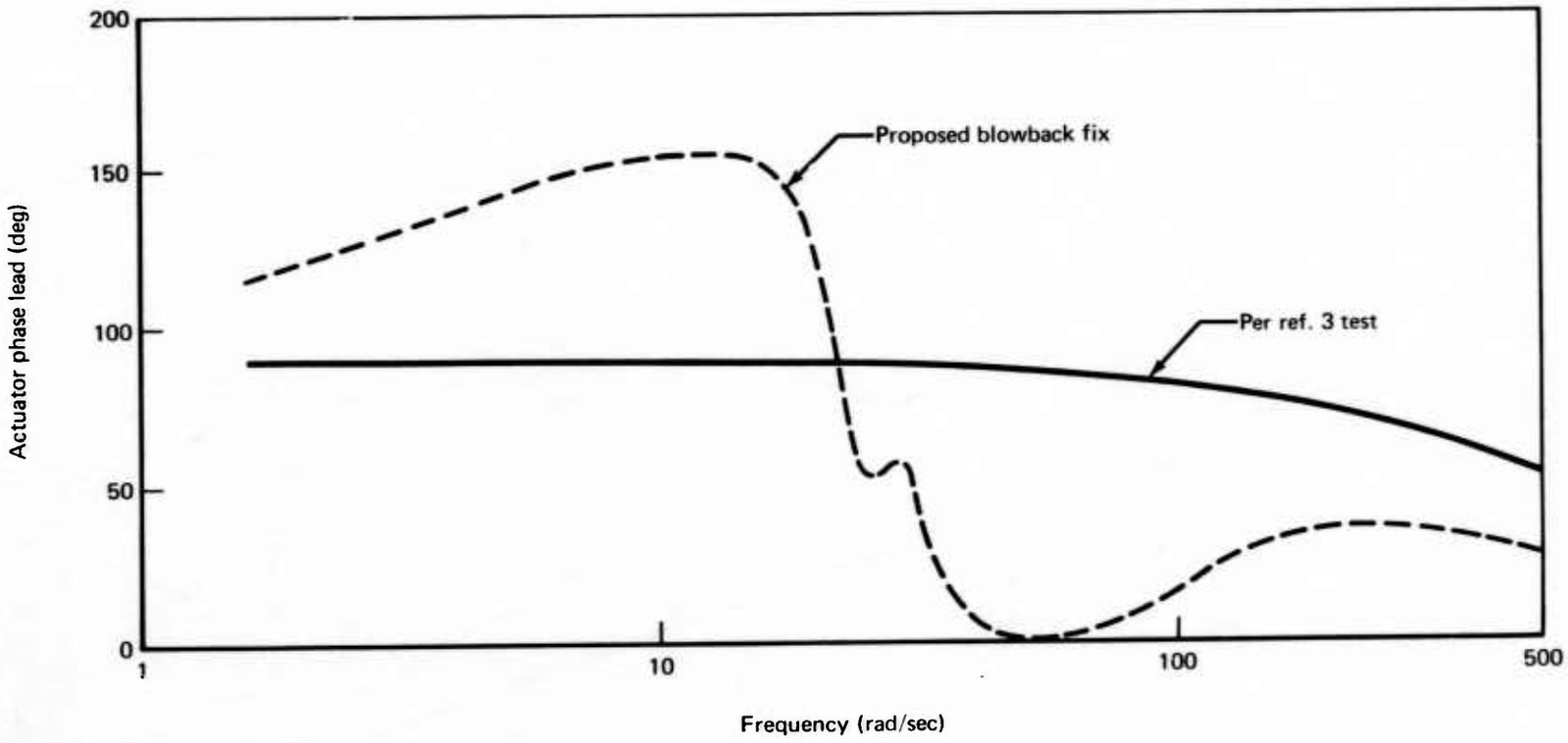

FIGURE 13.–HORIZONTAL STABILIZER ACTUATOR PHASE ANGLE, BLOWBACK CONDITION

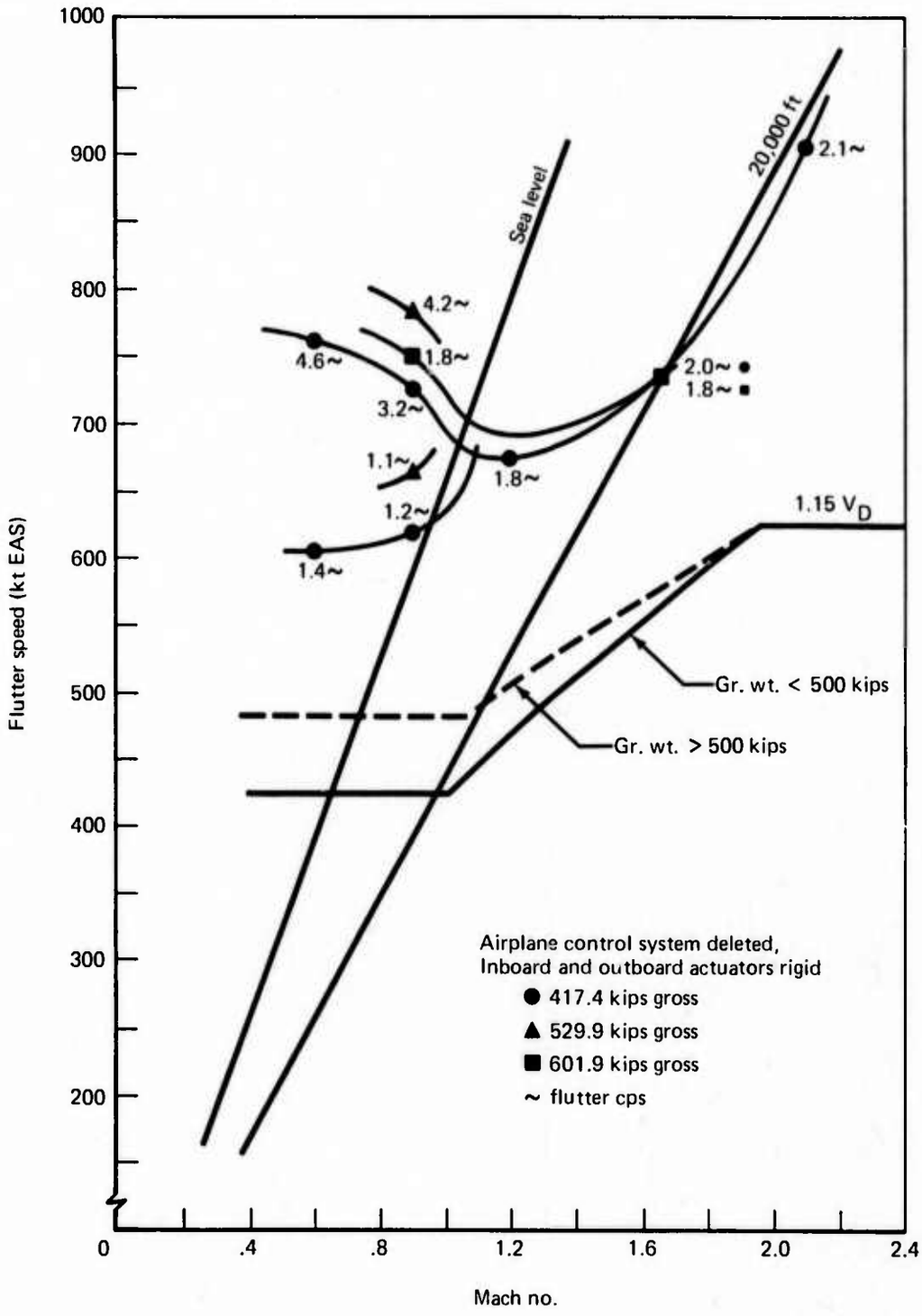

FIGURE 14.–SYMMETRIC HORIZONTAL STABILIZER FLUTTER BOUNDARIES, ACTUATORS RIGID

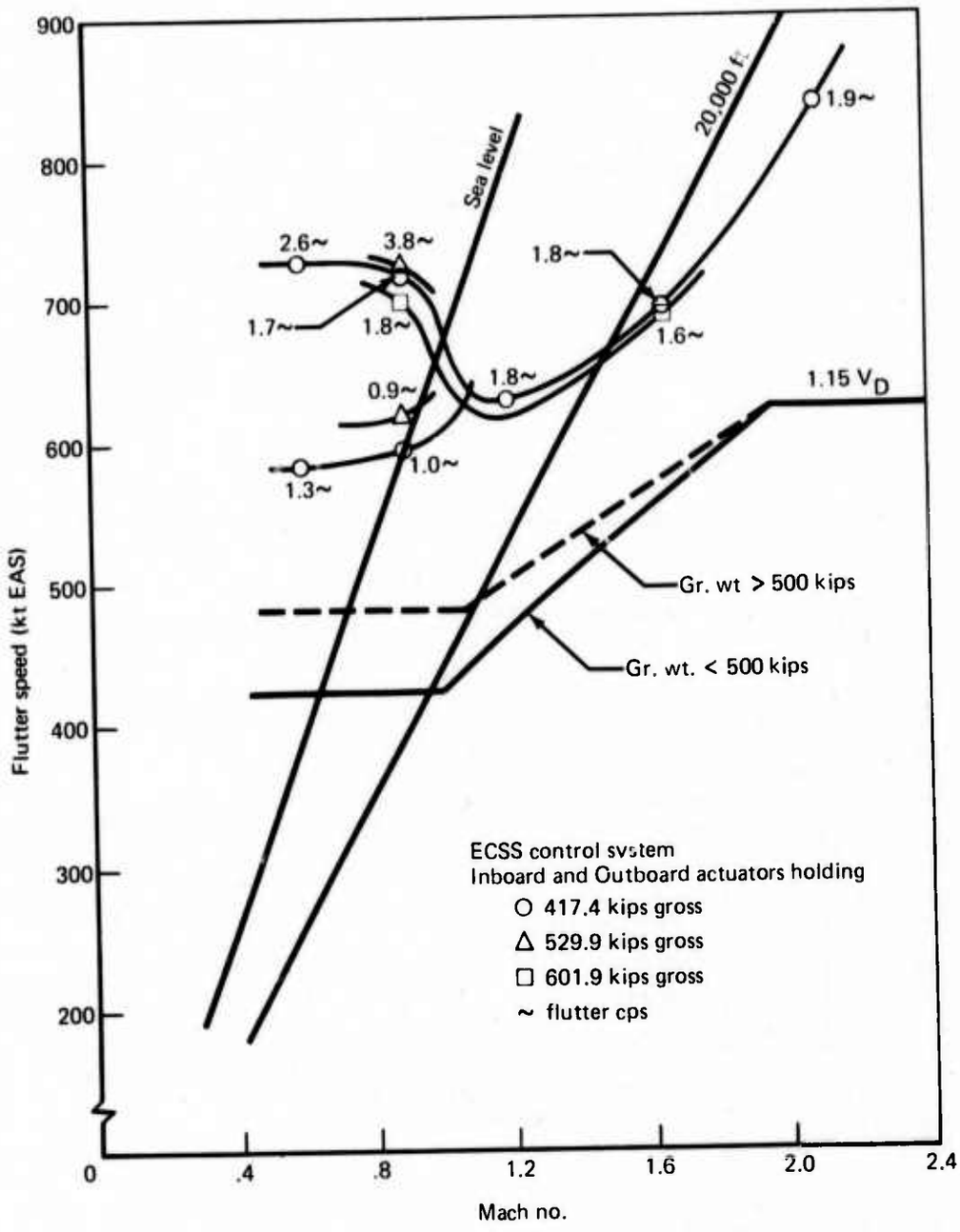

FIGURE 15.–SYMMETRIC HORIZONTAL STABILIZER FLUTTER BOUNDARIES, ACTUATORS HOLDING

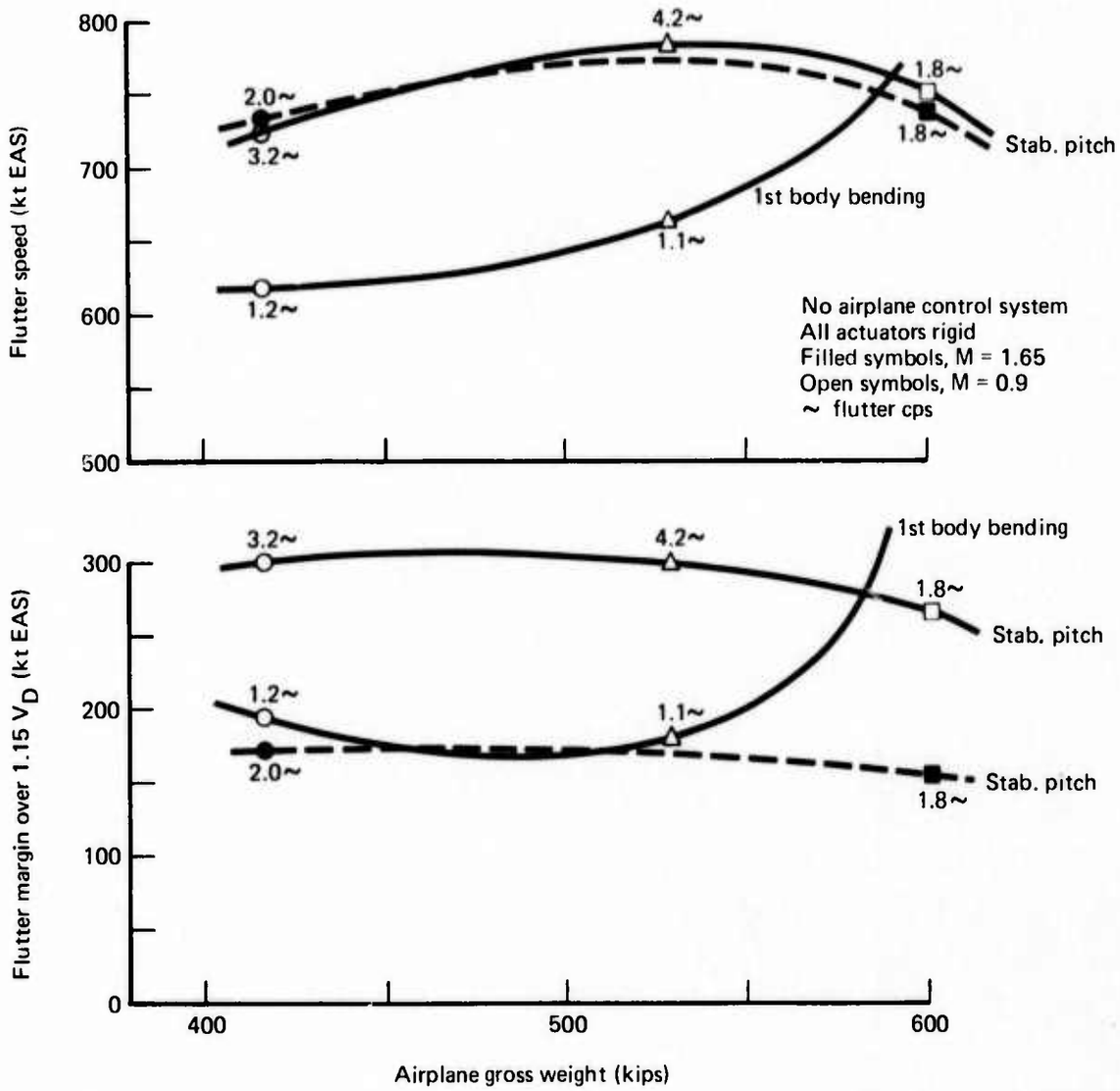

FIGURE 16.–AIRPLANE GROSS WEIGHT EFFECTS ON SYMMETRIC HORIZONTAL STABILIZER FLUTTER

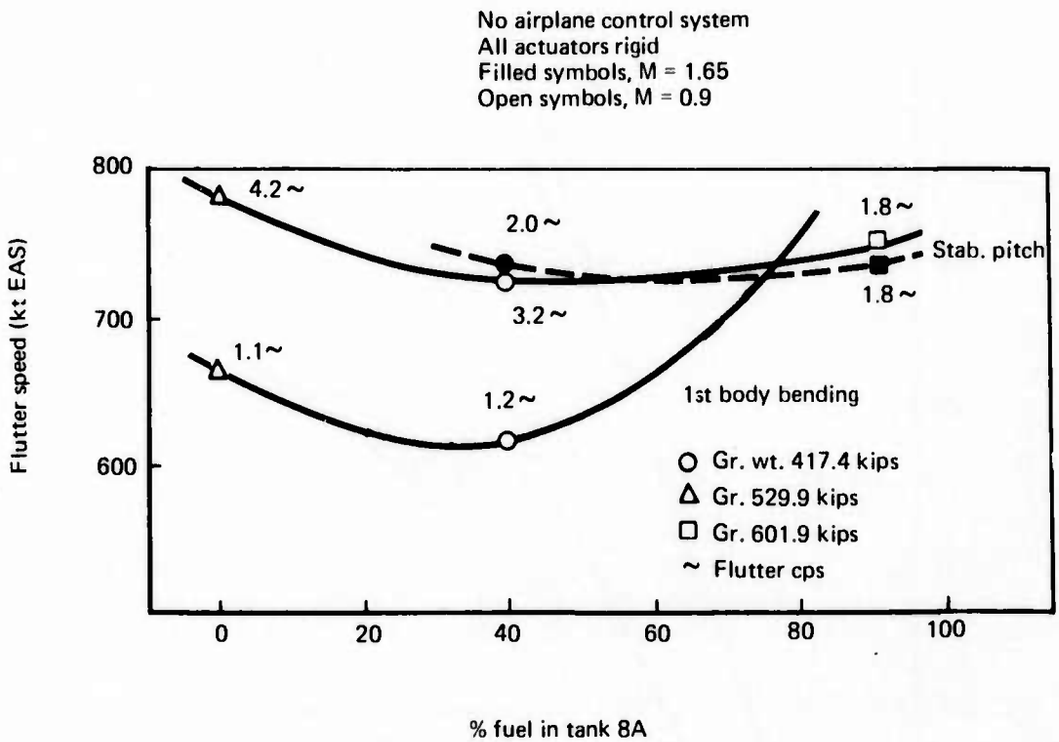

FIGURE 17.–STABILIZER FLUTTER SPEED VARIATION WITH TANK 8A FUEL

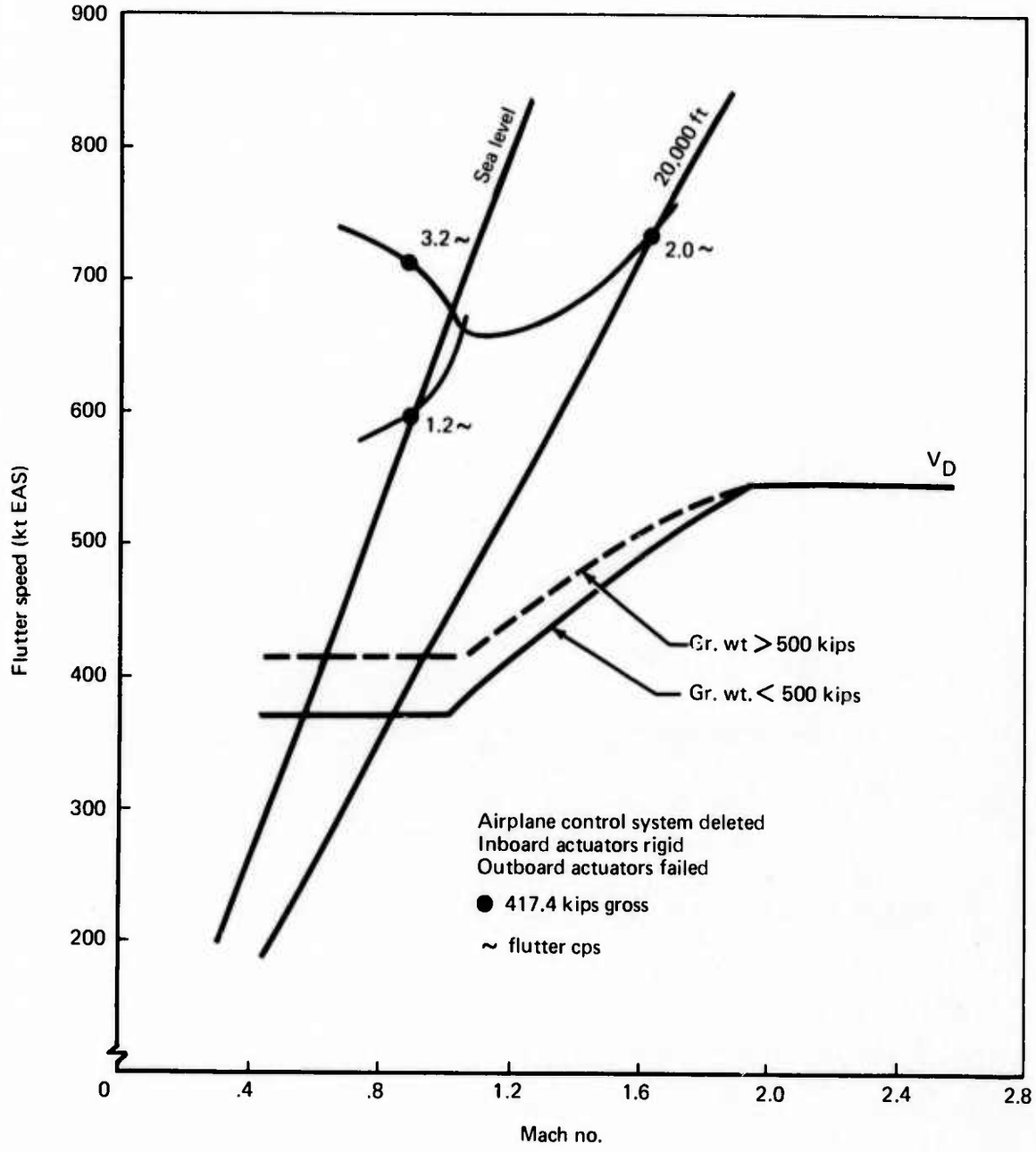

FIGURE 18.–HORIZONTAL STABILIZER FLUTTER BOUNDARY, FAILED AND RIGID ACTUATORS

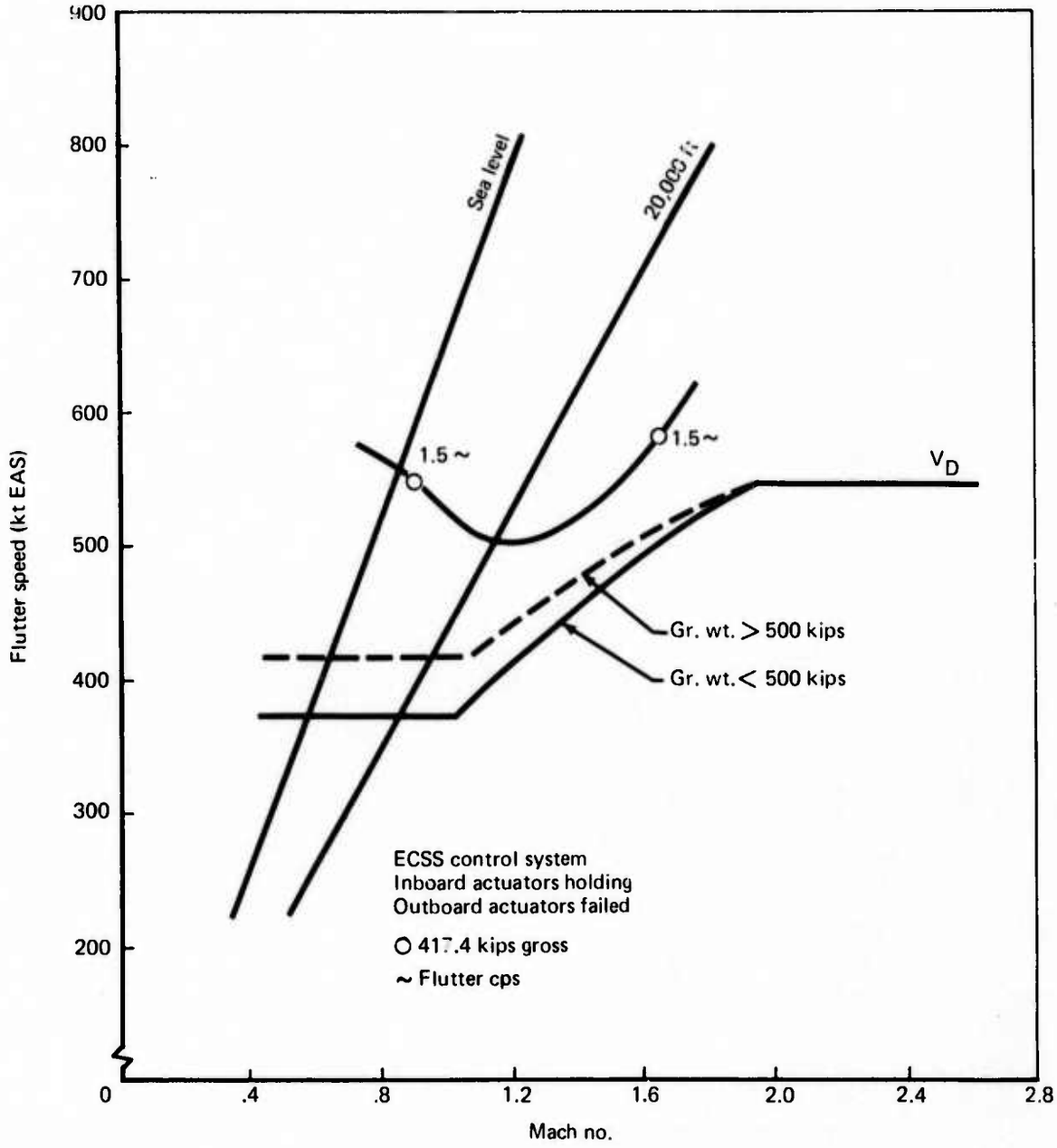

FIGURE 19.–SYMMETRIC HORIZONTAL STABILIZER FLUTTER BOUNDARY, FAILED AND HOLDING ACTUATORS

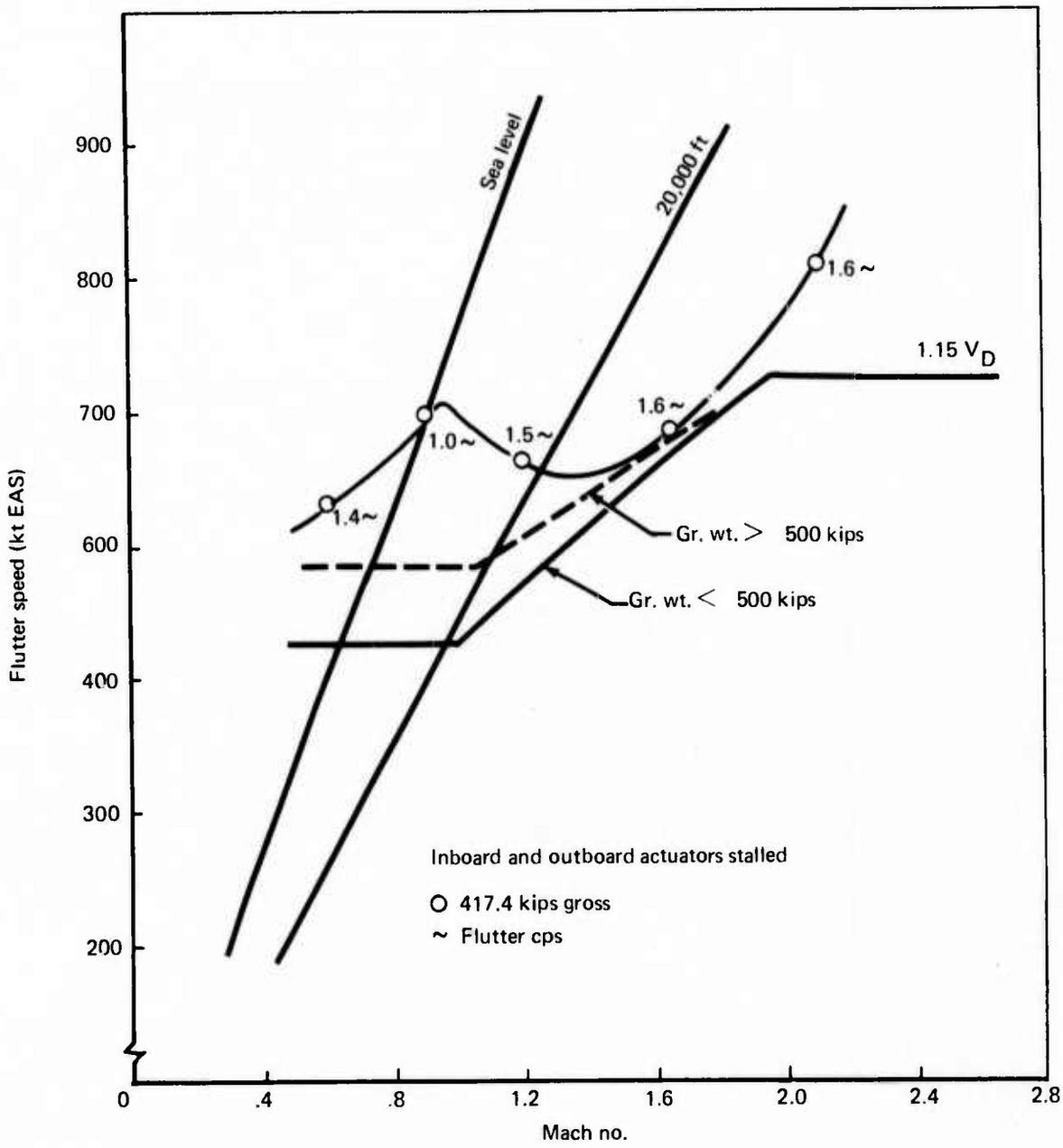

FIGURE 20.–SYMMETRIC HORIZONTAL STABILIZER FLUTTER BOUNDARY, ACTUATORS STALLED

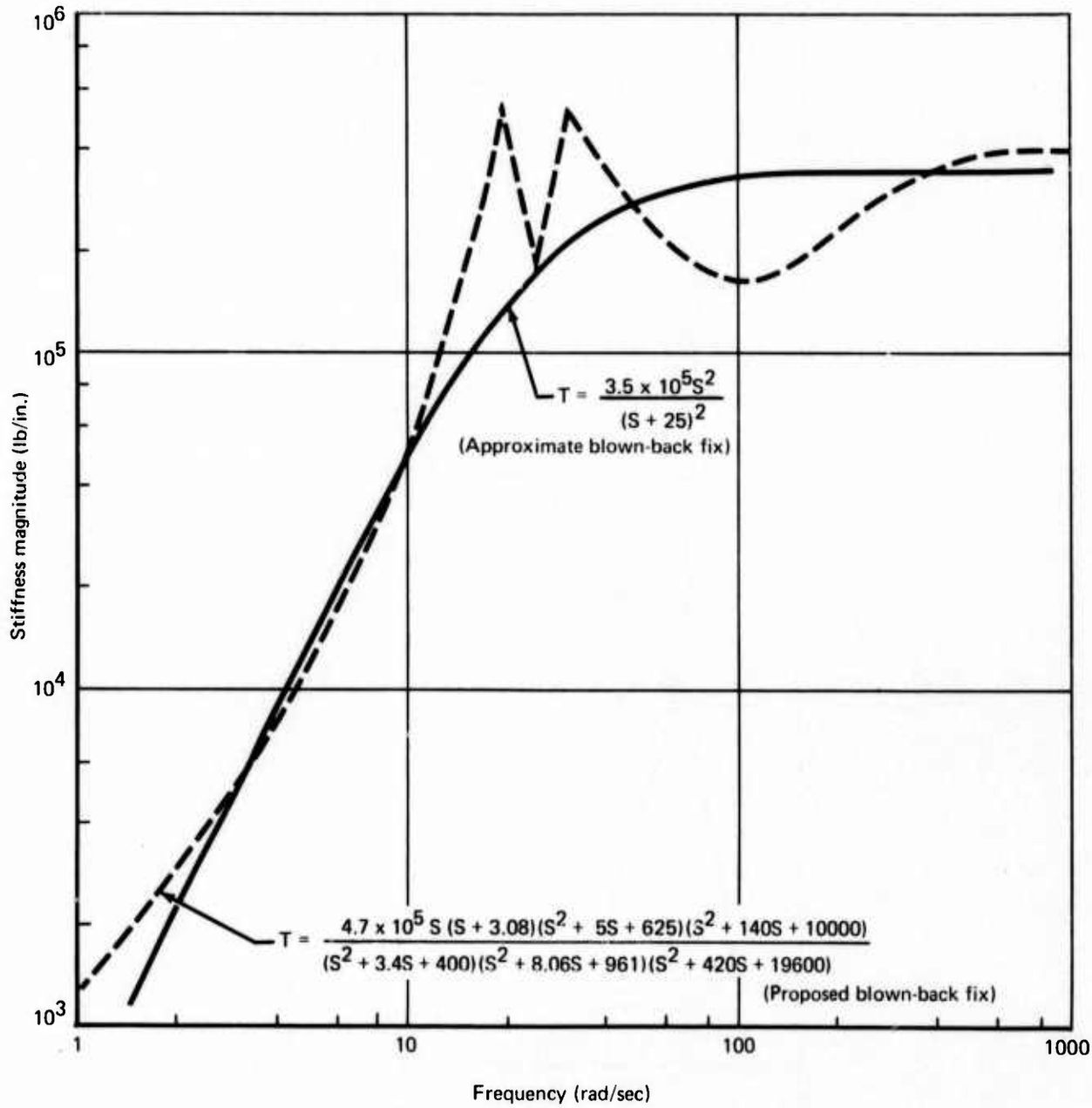

FIGURE 21.—TRANSFER FUNCTION APPROXIMATION, ACTUATORS BLOWN BACK

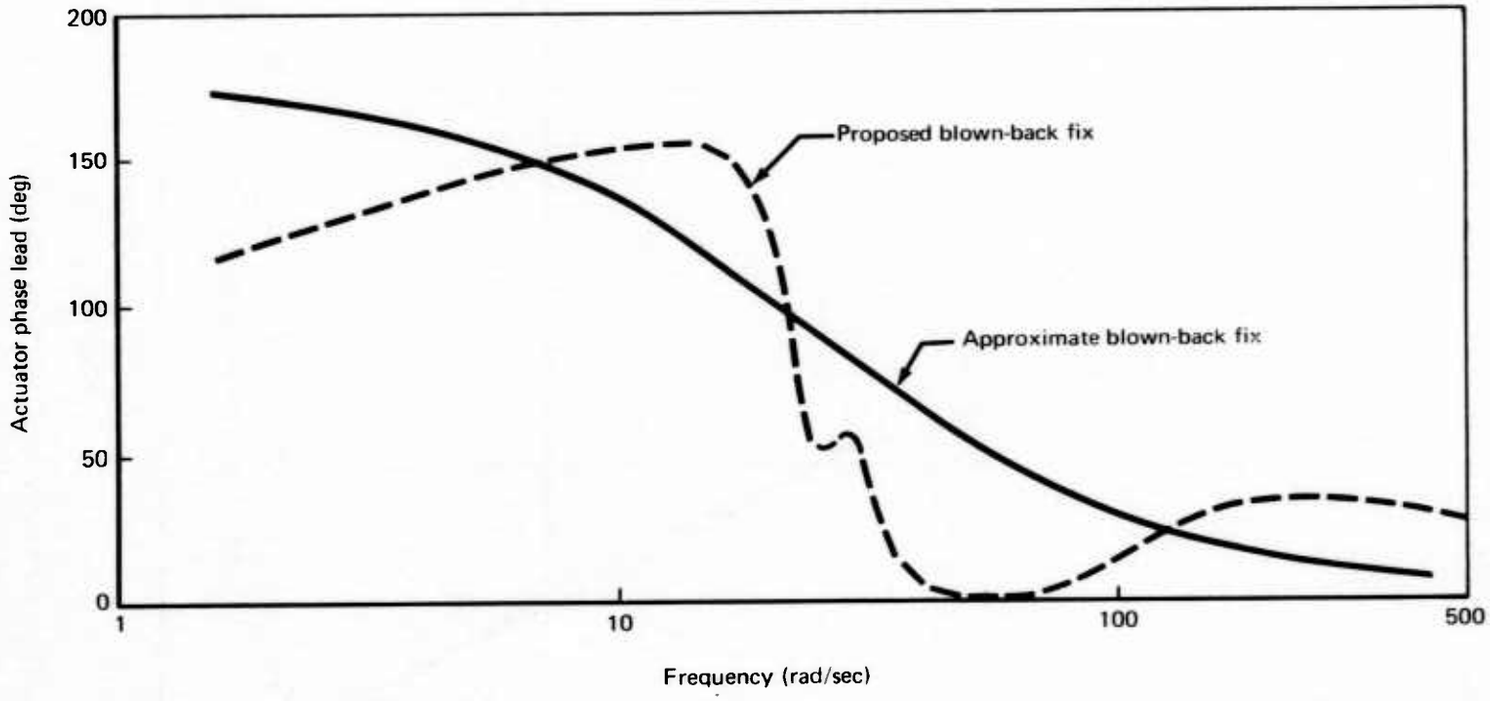

FIGURE 22.–TRANSFER FUNCTION APPROXIMATION, ACTUATORS BLOWN BACK

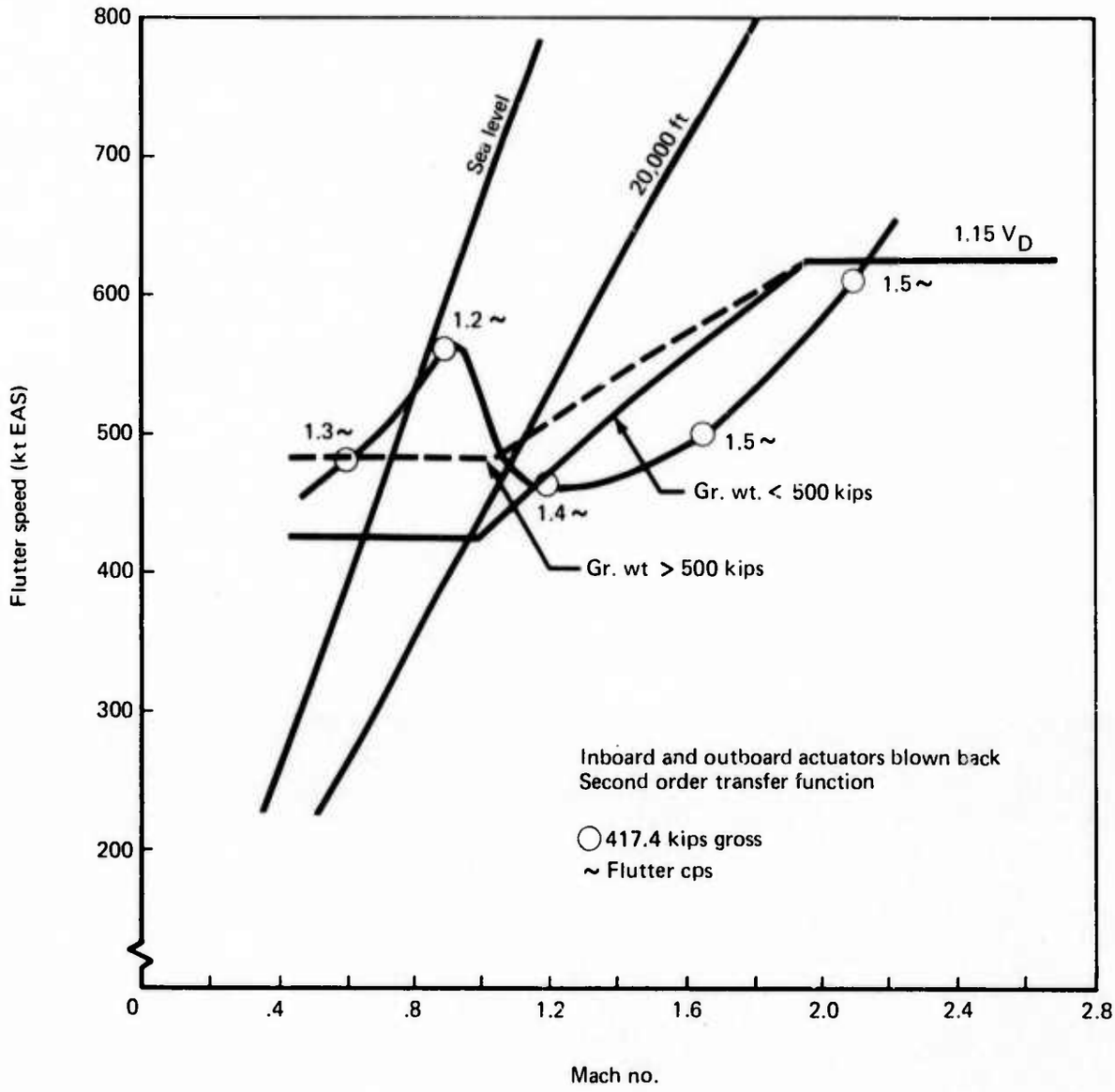

FIGURE 23.–SYMMETRIC HORIZONTAL STABILIZER FLUTTER BOUNDARY, ACTUATORS BLOWN BACK

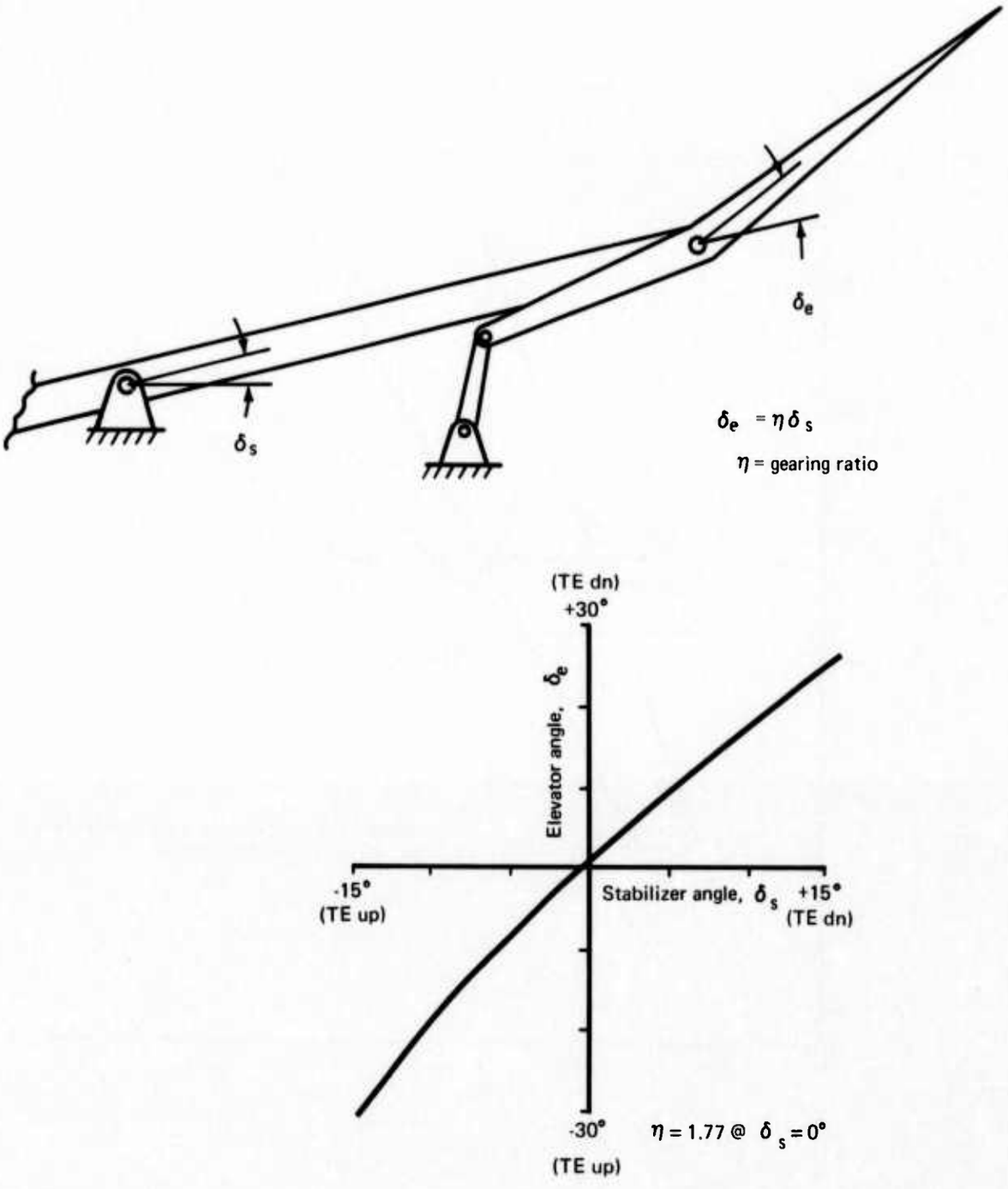

FIGURE 24.--GEARED ELEVATOR DESIGN

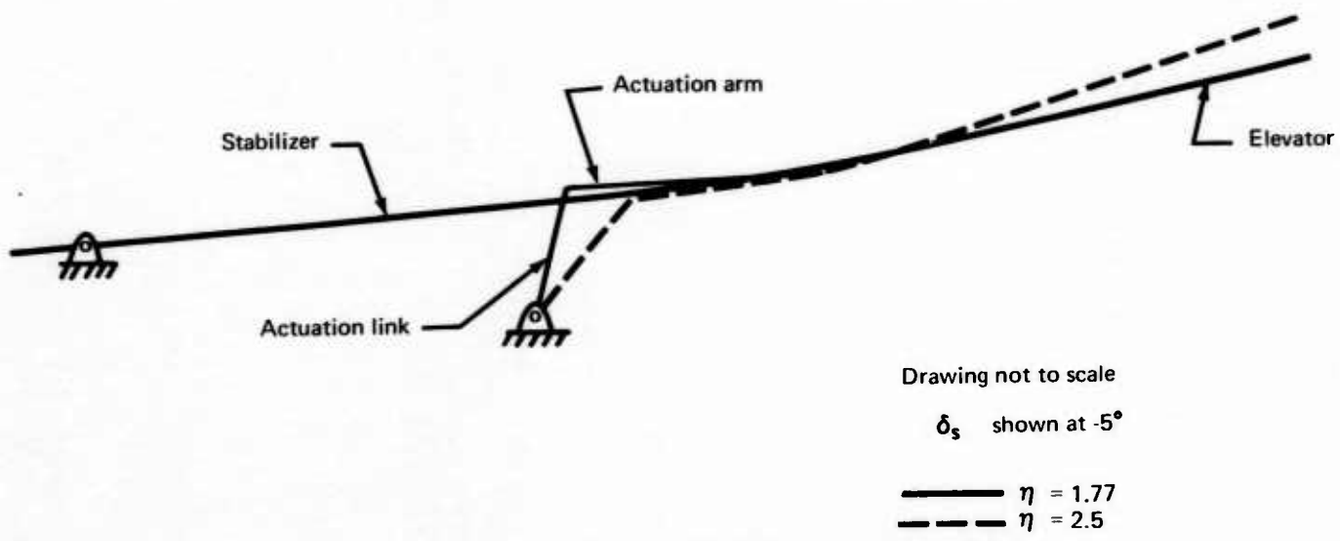

FIGURE 25.—GEOMETRY CHANGES TO PRODUCE GEARING RATIO CHANGE

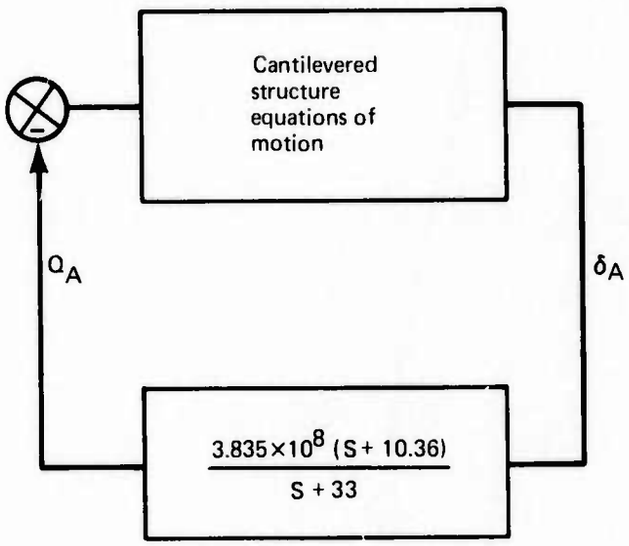

Transfer function varies with actuator condition. Single, holding actuator shown acting at a distance of 33.1 in. about hinge ($\delta_s = 0$)

δ_A = actuator linear displacement divided by torque arm (33.1 in.)

Q_A = actuator force multiplied by torque arm (33.1 in.)

FIGURE 26.–CONTROL SYSTEM USED FOR GEARED ELEVATOR FLUTTER ANALYSES

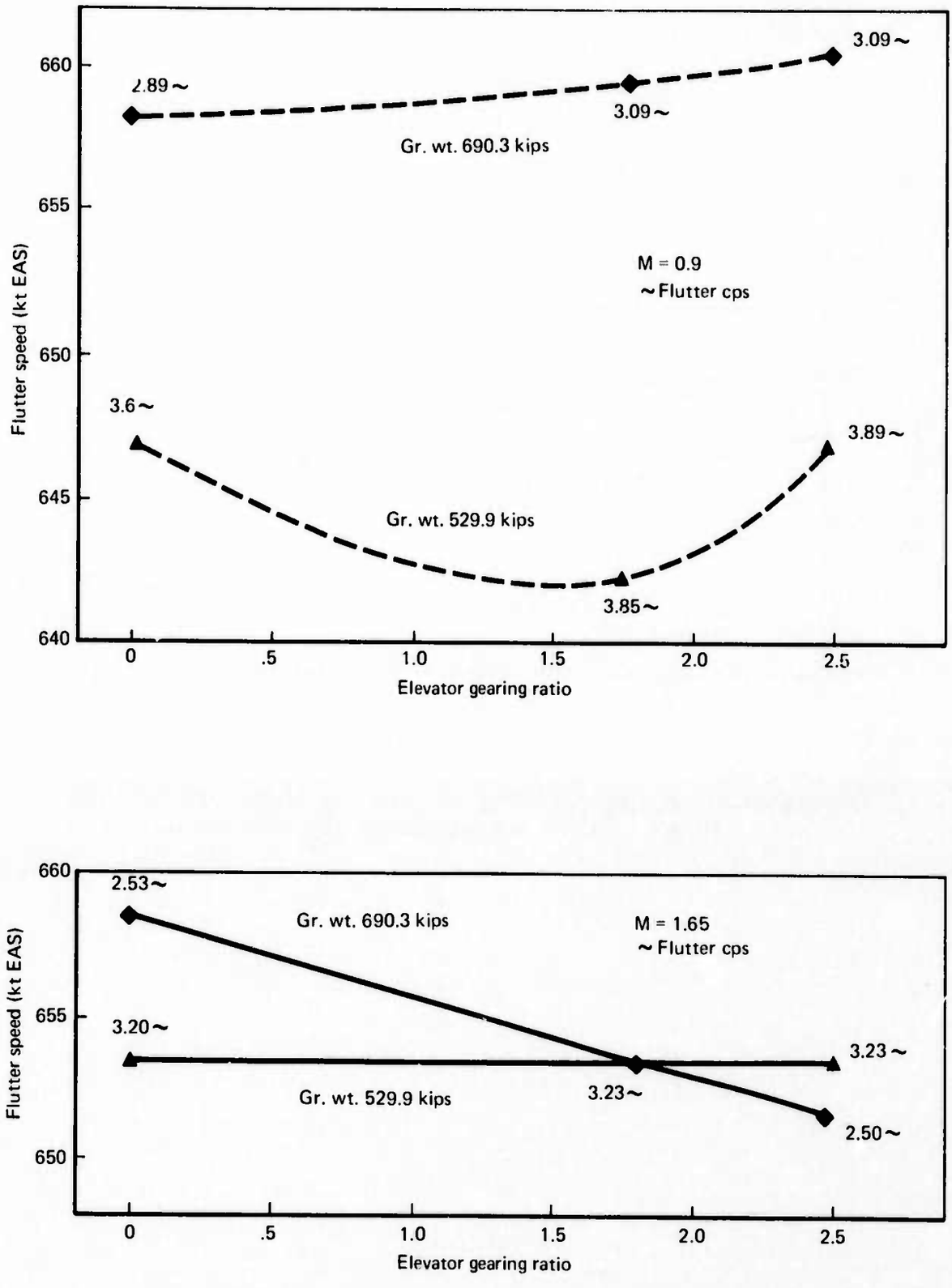

FIGURE 27.–EFFECT OF ELEVATOR GEARING ON HORIZONTAL STABILIZER FLUTTER, ACTUATORS RIGID

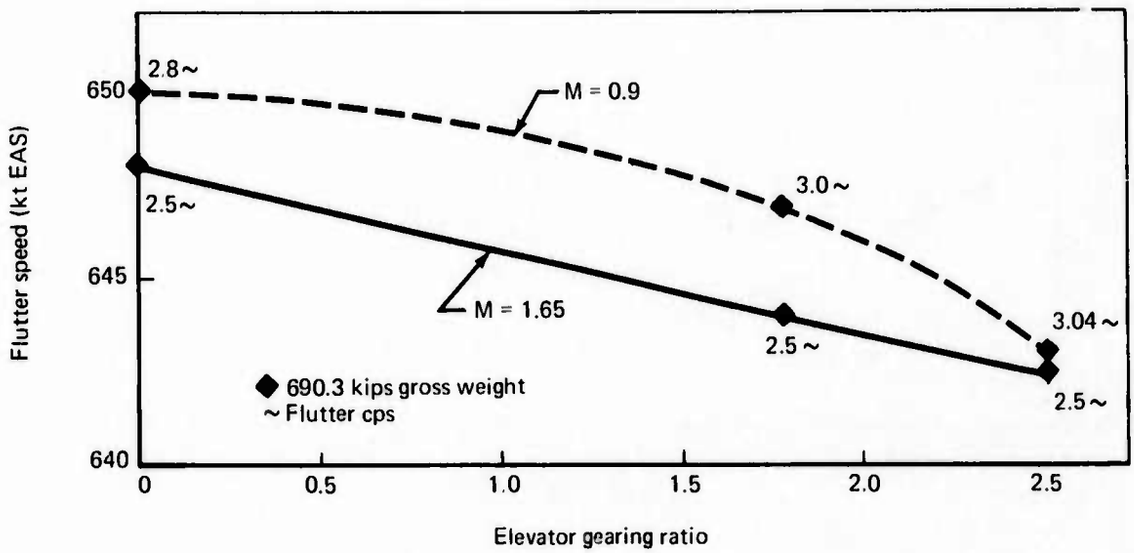

FIGURE 28.–EFFECT OF ELEVATOR GEARING ON STABILIZER FLUTTER, OUTBOARD ACTUATORS FAILED, INBOARD RIGID

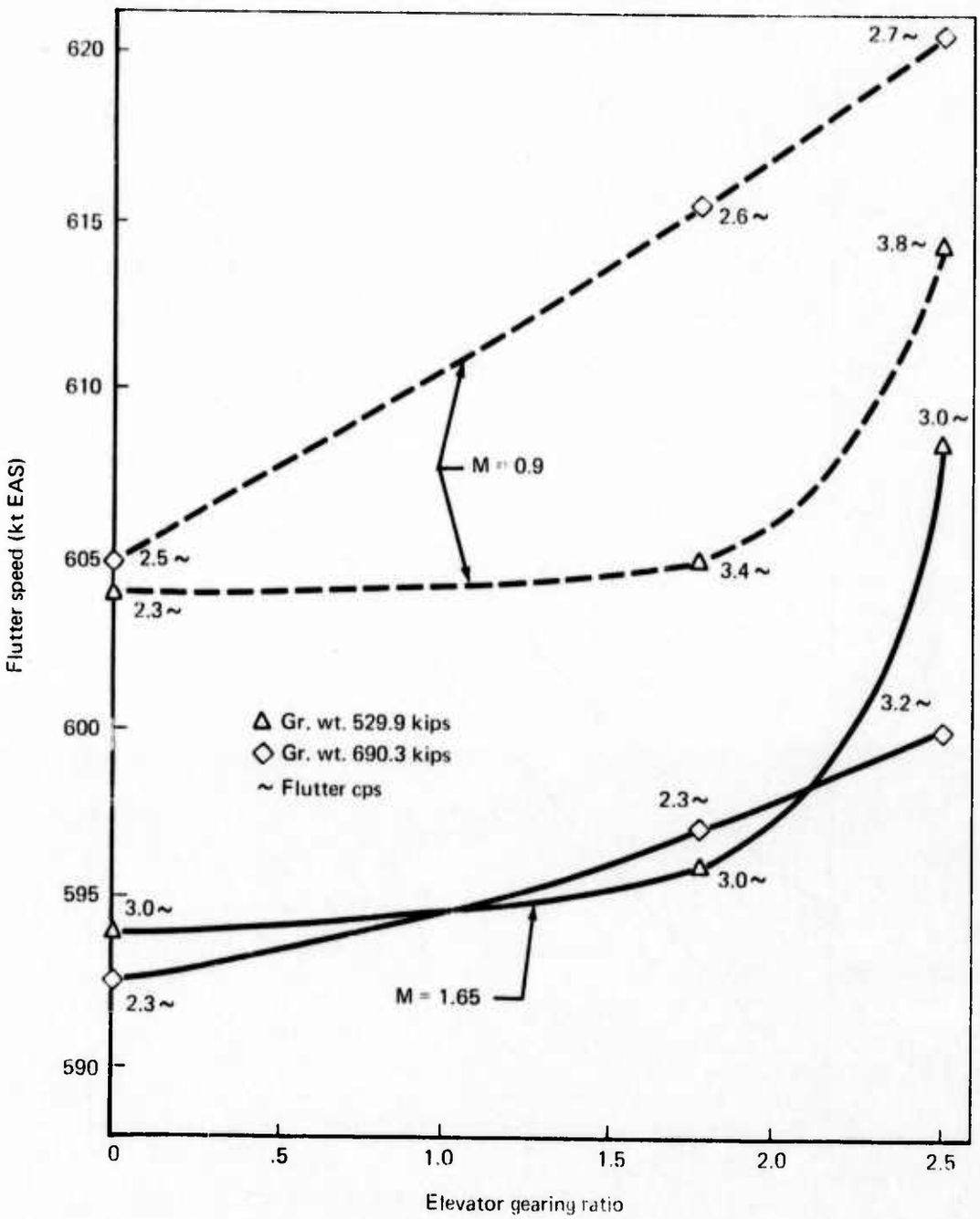

FIGURE 29.–EFFECT OF ELEVATOR GEARING ON STABILIZER FLUTTER, ACTUATORS HOLDING

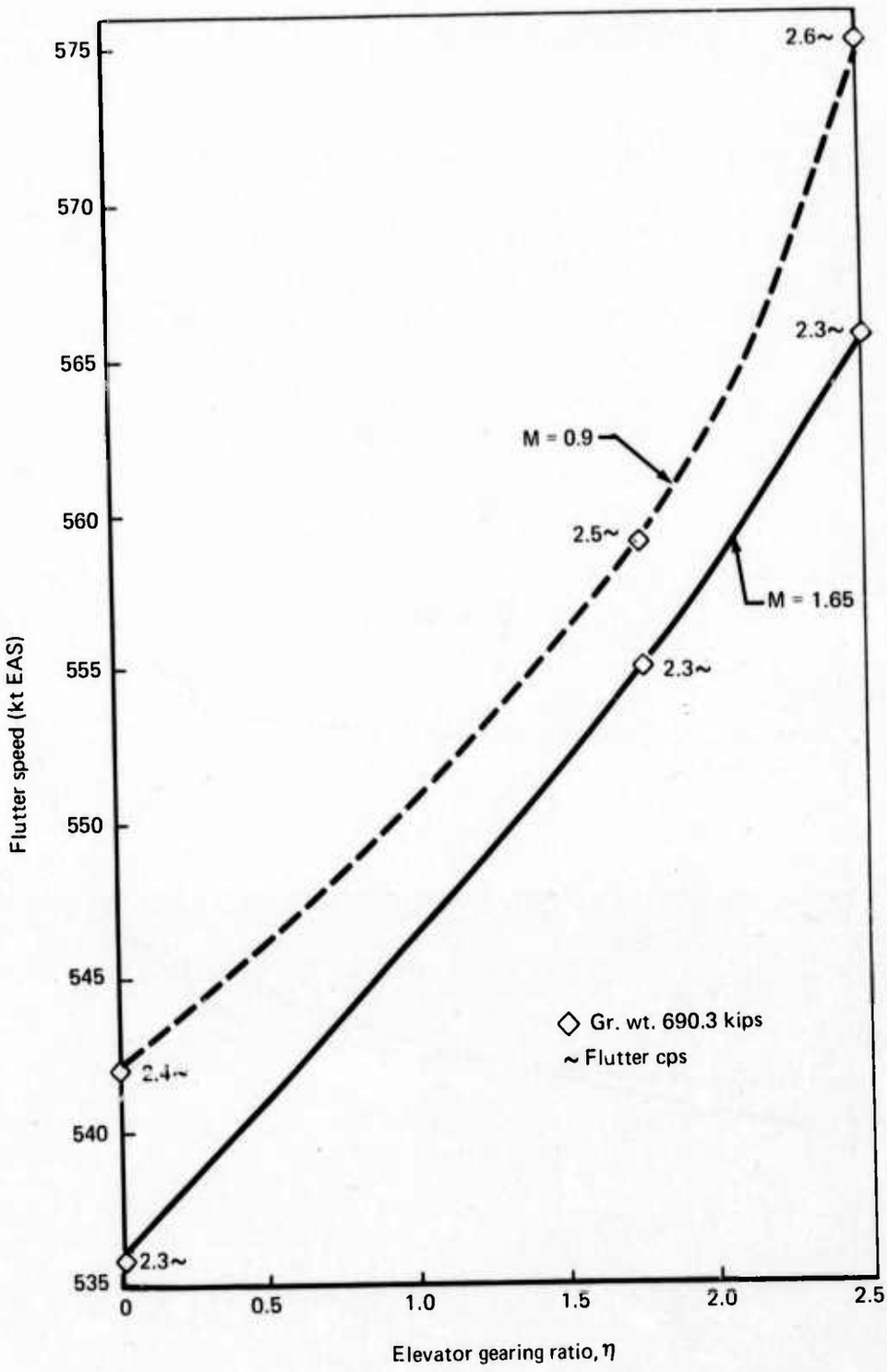

FIGURE 30.—EFFECT OF ELEVATOR GEARING ON STABILIZER FLUTTER, OUTBOARD ACTUATORS FAILED, INBOARD HOLDING

APPENDIX A

EQUATIONS OF MOTION DEVELOPMENT

The theoretical development of the equations of motion for an elastic airplane structure including a stiffness coupled actuator mode is given as follows:

Assume a symmetric analysis, for which the Lagrange equations can be written as

$$\frac{d}{dt}\left(\frac{\partial T}{\partial \dot{q}}\right) = \sum_i Z_i \frac{\partial z}{\partial q}i \tag{A1}$$

where:

T = kinetic energy

Z_i = sum of structural stiffness force plus external aerodynamic forces

z_i = total displacement of panel i

q = generalized coordinate

Writing out the above expressions.

$$T = \sum_i \frac{1}{2} m_i \dot{z}_i^2 \tag{A2}$$

$$Z_i = -\sum_j k_{ij} z_j^E - \frac{1}{2}\rho U^2 \sum_j a_{ij} \alpha_j \tag{A3}$$

where

$$\alpha_j = \frac{\dot{z}_j}{U} - \left(\frac{\partial z}{\partial x}\right)_j \tag{A4}$$

a_{ij} = aerodynamic influence coefficients

k_{ij} = stiffness matrix for structure

z_i^E = elastic component of total displacement

In terms of generalized coordinates, we can write

$$z_i = \phi_i q \tag{A5}$$

Assume, initially, that we are considering only the elastic modes of the structure, i.e., no actuator mode is yet included. Therefore,

$$z_i = z_i^E \tag{A6}$$

Introducing the superscript E in all terms to denote the elastic components only, we can write the Lagrange equations as:

$$\frac{d}{dt}\left[\frac{\partial\left(\sum_i \frac{1}{2} m_i \dot{z}_i^{E\,2}\right)}{\partial \dot{q}^E}\right] = -\sum_i \sum_j k_{ij} z_j^E \frac{\partial z_i^E}{\partial q^E} - \frac{1}{2}\rho U^2 \sum_i \sum_j a_{ij} \left[\frac{\dot{z}_j^E}{U} - \left(\frac{\partial z}{\partial x}\right)_j^E\right] \frac{\partial z_i^E}{\partial q^E} \quad \text{(A7)}$$

Eliminating the subscripts and writing in matrix form,

$$\{z^E\} = [\phi^E]\{q^E\}$$

and

$$\left\{\frac{\partial z^E}{\partial x}\right\} = z'^E = [\phi'^E]\, q^E$$

the above equation becomes,

$$[\phi^E]^T [m] [\phi^E] \{\ddot{q}^E\} = -[\phi^E]^T [k] [\phi^E] \{q^E\} - \frac{1}{2}\rho U [\phi^E]^T [a] [\phi^E] \{\dot{q}^E\} + \frac{1}{2}\rho U^2 [\phi^E]^T [a] [\phi'^E] \{q^E\} \quad \text{(A8)}$$

Equation (A8) is recognized as the usual equation of motion for an aeroelastic structure.

Let us include now an additional actuator mode. The effect of this mode is to create additional deflections, z_i^A, so that

$$z_i \neq z_i^E \quad \text{(A9)}$$

but,

$$z_i = z_i^E + z_i^A \quad \text{(A10)}$$

In terms of an actuator generalized coordinate, δ_A, we can write

$$z_i^A = \phi_i^A \delta_A \quad \text{(A11)}$$

As stated in (A9) above,

$$\{z\} \neq [\phi^E]\{q^E\} \quad \text{(A12)}$$

but we can say that

$$\{z\} = [\phi^E]\{\bar{q}\} \tag{A13}$$

where $\{\bar{q}\}$ is now a new set of generalized coordinates that relate the elastic structure mode shapes to the total displacements of the structure nodes.

Extend the bar notation to all terms to denote the inclusion of the actuator mode, so that (A13) becomes

$$\{\bar{z}\} = [\phi^E]\{\bar{q}\} \tag{A14}$$

Lagrange's equations now appear as,

$$\frac{d}{dt}\left[\frac{\partial\left(\sum_i \frac{1}{2} m_i \dot{\bar{z}}_i^2\right)}{\partial \dot{\bar{q}}}\right] = -\sum_i \sum_j k_{ij}\left(\bar{z}_j - z_j{}^A\right)\frac{\partial\left(\bar{z}_i - z_i{}^A\right)}{\partial \bar{q}} - \sum_i \sum_j \frac{1}{2}\rho U^2 a_{ij}\left[\frac{\dot{\bar{z}}}{U} - \left(\frac{\partial \bar{z}}{\partial x}\right)_j\right]\frac{\partial \bar{z}_i}{\partial \bar{q}} \tag{A15}$$

Since δ_A is now another generalized coordinate, another equation of motion is produced:

$$\begin{aligned}\frac{d}{dt}\left[\frac{\partial\left(\sum_i \frac{1}{2} m_i \dot{\bar{z}}_i^2\right)}{\partial \dot{\delta}_A}\right] &= -\sum_i \sum_j k_{ij}\left(\bar{z}_j - z_j{}^A\right)\frac{\partial\left(\bar{z}_i - z_i{}^A\right)}{\partial \delta_A} \\ &\quad - \sum_i \sum_j \frac{1}{2}\rho U^2 a_{ij}\left[\frac{\dot{\bar{z}}}{U} - \left(\frac{\partial \bar{z}}{\partial x}\right)_j\right]\frac{\partial \bar{z}_i}{\partial \delta_A} + Q_A\end{aligned} \tag{A16}$$

In matrix form, equations (A15) and (A16) may be combined as

$$\begin{aligned}&\left[\begin{array}{c}\phi^E \\ \hline 0\end{array}\right]^T [m] \left[\phi^E \,\vdots\, 0\right]\left\{\begin{array}{c}\ddot{\bar{q}} \\ \hline \ddot{\delta}_A\end{array}\right\} + \frac{1}{2}\rho U \left[\begin{array}{c}\phi^E \\ \hline 0\end{array}\right]^T [a] \left[\phi^E \,\vdots\, 0\right]\left\{\begin{array}{c}\dot{\bar{q}} \\ \hline \dot{\delta}_A\end{array}\right\} + \left[\begin{array}{c}\phi^E \\ \hline -\phi^A\end{array}\right]^T [k] \left[\phi^E \,\vdots\, -\phi^A\right]\left\{\begin{array}{c}\bar{q} \\ \hline \delta_A\end{array}\right\} \\ &-\frac{1}{2}\rho U^2 \left[\begin{array}{c}\phi^E \\ \hline 0\end{array}\right]^T [a] \left[\phi' E \,\vdots\, 0\right]\left\{\begin{array}{c}\bar{q} \\ \hline \delta_A\end{array}\right\} = \left\{\begin{array}{c}0 \\ \hline Q_A\end{array}\right\}\end{aligned} \tag{A17}$$

Note that the coupling between the elastic modes and the actuator mode occurs in the generalized stiffness matrix, thus giving rise to the term "stiffness coupled formulation."

Equation (A17) can be written in terms of unsteady aerodynamics for use in flutter studies.

$$\left[\begin{array}{c|c}M & 0 \\ \hline 0 & 0\end{array}\right]\left\{\begin{array}{c}\ddot{\bar{q}} \\ \hline \ddot{\delta}_A\end{array}\right\} + \left[\begin{array}{c|c}K & -[\phi^E]^T [k] [\phi^A] \\ \hline -[\phi^A]^T [k] [\phi^E] & [\phi^A]^T [k] [\phi^A]\end{array}\right]\left\{\begin{array}{c}\bar{q} \\ \hline \delta_A\end{array}\right\} + \frac{\omega^2}{\Gamma}\left[\begin{array}{c|c}A & 0 \\ \hline 0 & 0\end{array}\right]\left\{\begin{array}{c}\bar{q} \\ \hline \delta_A\end{array}\right\} = \left\{\begin{array}{c}0 \\ \hline Q_A\end{array}\right\} \tag{A18}$$

where:

$$M = \left[\phi^E\right]^T [m] \left[\phi^E\right]$$

$$K = \left[\phi^E\right]^T [k] \left[\phi^E\right] \qquad \text{(A18)}$$

$$A = \left[\phi^E\right]^T [a] \left[\frac{i\omega}{U}\phi^E - \phi'^E\right]$$

We can make Q_A a generalized coordinate and introduce structural damping to the equations of motion in the usual manner. Equation (A18) then becomes

$$\left[\begin{array}{c|c|c} M & 0 & 0 \\ \hline 0 & 0 & 0 \end{array}\right]\left\{\begin{array}{c} \ddot{\bar{q}} \\ \hline \ddot{\delta}_A \\ \hline \ddot{Q}_A \end{array}\right\} + \left[\begin{array}{c|c|c} K(1+ig) & K_{12} & 0 \\ \hline K_{21} & K_{22} & -1.0 \end{array}\right]\left\{\begin{array}{c} \bar{q} \\ \hline \delta_A \\ \hline Q_A \end{array}\right\} + \frac{\omega^2}{\Gamma}\left[\begin{array}{c|c|c} A & 0 & 0 \\ \hline 0 & 0 & 0 \end{array}\right]\left\{\begin{array}{c} \bar{q} \\ \hline \delta_A \\ \hline Q_A \end{array}\right\} = \{0\} \qquad \text{(A19)}$$

where:

$$K_{12} = -\left[\phi^E\right]^T [k] \left[\phi^A\right]$$

$$K_{21} = -\left[\phi^A\right]^T [k] \left[\phi^E\right]$$

$$K_{22} = \left[\phi^A\right]^T [k] \left[\phi^A\right]$$

The control system feedback transfer function relating the actuator torque Q_A and displacement δ_A is generally of the form:

where:

$$T(s) = \frac{Q_A}{\delta_A} = \frac{C_2 (S + \omega_1)}{S + \omega_2}$$

C_2, ω_1, ω_2 = parameters of the system design

S = Laplace transform operator

In order to merge the control system equation with the equations of motion, it is necessary to transform the equations of motion, (A19), giving

$$\left[\begin{array}{c|c|c} M & 0 & 0 \\ \hline 0 & 0 & 0 \end{array}\right] S^2 + \left[\begin{array}{c|c|c} K(1+ig) & K_{12} & 0 \\ \hline K_{21} & K_{22} & -1.0 \end{array}\right] + \frac{\omega^2}{\Gamma}\left[\begin{array}{c|c|c} A & 0 & 0 \\ \hline 0 & 0 & 0 \end{array}\right] = [0] \qquad \text{(A20)}$$

The control system transfer function can now be merged with the equations of motion to form:

$$\begin{bmatrix} M & 0 & 0 \\ 0 & 0 & 0 \\ 0 & 0 & 0 \end{bmatrix} S^2 + \begin{bmatrix} 0 & 0 & 0 \\ 0 & 0 & 0 \\ 0 & -C_2 & -1.0 \end{bmatrix} S + \begin{bmatrix} K(1+ig) & K_{12} & 0 \\ K_{21} & K_{22} & -1.0 \\ 0 & -C_2\omega_1 & -\omega_2 \end{bmatrix} + \frac{\omega^2}{V^2} \begin{bmatrix} A & 0 & 0 \\ 0 & 0 & 0 \\ 0 & 0 & 0 \end{bmatrix} = 0 \qquad \text{(A21)}$$

Simplifying the notation,

$$[B]\, S^2 + [C]\, S + [D] + \frac{\omega^2}{V^2} [E] = 0 \qquad \text{(A22)}$$

This is the equation to be solved for flutter instabilities. Note, however, that both S and ω are unknown complex variables. If we restrict our examination of the solution to the vicinity of the imaginary axis ($\sigma = 0$ where $S = \sigma + i\omega$) we can write equations (A22) as

$$\left[[B] - \frac{1}{V^2}[E]\right] S^2 + [C]\, S + [D] = 0 \qquad \text{(A23)}$$

which is then rooted for S. From these roots, flutter velocity, frequency, and damping values can be obtained.

f_f = flutter frequency = $\frac{1}{2\pi}$ ABS (ROOT)

ζ = damping = REAL (ROOT)/$2\pi f_f$

g = -2.0 (ζ) (for small damping)

V_f = flutter velocity = $\frac{2\pi b_r f_f}{k}$

where k is the reduced frequency associated with the airforce matrix [E].

REFERENCES

1. M. C. Redman, W. S. Rowe, and B. A. Winther, *Prediction of Unsteady Aerodynamic Loadings Caused by Trailing Edge Control Surface Motions in Subsonic Compressible Flow*, NASA CR-112015, June 1974.

2. J. M. Ii, C. T. Borland, and J. R. Hogley, *Prediction of Unsteady Aerodynamic Loadings of Non-Planar Wings and Wing-Tail Configurations in Supersonic Flow*, AFFDL-TR-71-108, August 1971.

3. L. R. Appleford, M. L. Beattie, C. W. King, E. L. Maylor, and D. R. Ryder, *Test and Analysis of a Quadruple Redundant Horizontal Stabilizer Actuation System, SST Technology Follow-On Program—Phase I*, FAA-SS-72-70 (Boeing document D6-60270), April 1972.

4. Support Data for the Flutter Analysis of an All-Movable Horizontal Tail with Geared Elevator on a Supersonic Transport, Boeing document D6-41848, 1974.